ARL-TR-8764 ● AUG 2019

DEVCOM ARMY RESEARCH LABORATORY

Surface Mechanical Attrition for Coating Adhesion, Mechanical Bonding, Corrosion Mitigation, and Wear Resistance: SERDP Project WP-2741 Final Report

by Heather Murdoch, Joseph Labukas, Denise Yin, and B Chad Hornbuckle

NOTICES

Disclaimers

The findings in this report are not to be construed as an official Department of the Army position unless so designated by other authorized documents.

Citation of manufacturer's or trade names does not constitute an official endorsement or approval of the use thereof.

Destroy this report when it is no longer needed. Do not return it to the originator.

ARL-TR-8764 ● AUG 2019

Surface Mechanical Attrition for Coating Adhesion, Mechanical Bonding, Corrosion Mitigation, and Wear Resistance: SERDP Project WP-2741 Final Report

by Heather Murdoch, Joseph Labukas, Denise Yin, and B Chad Hornbuckle
Weapons and Materials Research Directorate, CCDC Army Research Laboratory

REPORT DOCUMENTATION PAGE

Form Approved
OMB No. 0704-0188

1. REPORT DATE *(DD-MM-YYYY)*	2. REPORT TYPE	3. DATES COVERED (From - To)
August 2019	SERDP Final Report	1 February 2017–1 February 2018

4. TITLE AND SUBTITLE
Surface Mechanical Attrition for Coating Adhesion, Mechanical Bonding, Corrosion Mitigation, and Wear Resistance: SERDP Project WP-2741 Final Report

5a. CONTRACT NUMBER

5b. GRANT NUMBER

5c. PROGRAM ELEMENT NUMBER

6. AUTHOR(S)
Heather Murdoch, Joseph Labukas, Denise Yin, and B Chad Hornbuckle

5d. PROJECT NUMBER
WP-2741

5e. TASK NUMBER

5f. WORK UNIT NUMBER

7. PERFORMING ORGANIZATION NAME(S) AND ADDRESS(ES)
CCDC Army Research Laboratory
ATTN: FCDD-RLW-MF
Aberdeen Proving Ground, MD 21005

8. PERFORMING ORGANIZATION REPORT NUMBER
ARL-TR-8764

9. SPONSORING/MONITORING AGENCY NAME(S) AND ADDRESS(ES)
Strategic Environmental Research and Development Program
4800 Mark Center Drive, Suite 16F16
Alexandria, VA 22350-3605

10. SPONSOR/MONITOR'S ACRONYM(S)
WP-2741

11. SPONSOR/MONITOR'S REPORT NUMBER(S)
SERDP

12. DISTRIBUTION/AVAILABILITY STATEMENT
Distribution A: Approved for public release; distribution is unlimited.

13. SUPPLEMENTARY NOTES
ORCID ID: Heather Murdoch, 0000-0001-7710-0577

14. ABSTRACT
The objective of this work is to explore the feasibility of a novel severe surface plastic deformation process to simultaneously improve the corrosion resistance of the substrate while imparting desired surface chemistry and morphology. This limited scope project has two aims: 1) quantify the ways in which a gradient microstructure achieved through this method can enhance the corrosion resistance of a treated aluminum alloy substrate and 2) extend and develop this surface treatment to engender a surface alumina layer in single-step method without hazardous chemical processes. This limited scope program has shown the feasibility of the Surface Mechanical Alloying for Specialized Heterogeneity (SMASH) treatment to improve the corrosion response of aluminum alloy AA5083. The mechanism for this improvement—reduction of magnesium content into the depth of the substrate as a result of plastic deformation—is not one that has been observed before in other methods of severe plastic deformation applied to AA5083 and opens up new methods for improving sensitization behavior of aluminum–magnesium alloys. The SMASH process was successful in producing an alumina layer 20–100 μm thick on aluminum alloy substrates through a mechanical mixing approach that uses only powder as input and discard (e.g., no acid baths as hazardous waste). However, the coatings have a range of particle distribution and are morphologically very different from traditional anodized coatings. Significant further testing is necessary to determine how this would affect adhesion and wear.

15. SUBJECT TERMS
severe plastic deformation, sensitization, anodizing, aluminum alloys, Surface Mechanical Attrition Treatment, SMAT, Surface Mechanical Alloying for Specialized Heterogeneity, SMASH

16. SECURITY CLASSIFICATION OF:			17. LIMITATION OF ABSTRACT	18. NUMBER OF PAGES	19a. NAME OF RESPONSIBLE PERSON
a. REPORT	b. ABSTRACT	c. THIS PAGE			Heather Murdoch
Unclassified	Unclassified	Unclassified	UU	49	19b. TELEPHONE NUMBER (Include area code) (410) 306-0699

Standard Form 298 (Rev. 8/98)
Prescribed by ANSI Std. Z39.18

Contents

List of Figures

List of Tables

Executive Summary

Objective: The objective of this work is to explore the feasibility of a novel severe surface plastic deformation process to simultaneously improve the corrosion resistance of the substrate while imparting desired surface chemistry and morphology. This limited scope project has two aims: 1) quantify the ways in which a gradient microstructure achieved through this method can enhance the corrosion resistance of a treated aluminum (Al) alloy substrate and 2) extend and develop this surface treatment to engender a surface alumina layer in single-step method without hazardous chemical processes.

Technical Approach: Surface Mechanical Attrition Treatment (SMAT) is a relatively unexplored severe surface deformation process that produces a nanocrystalline/ultra-fine-grain layer of varying depth and gradient. Reduction in grain size can lead to enhanced corrosion resistance, and changes in compressive stress can improve pitting potentials and mitigate stress corrosion cracking. Additionally, the SMAT process offers the opportunity for both a large range of microstructural control and the opportunity for supplementary surface alloying. The severe plastic deformation imparted to the substrate surface from the SMAT process that engenders grain refinement can also reduce existing intermetallic/precipitate size—reducing localized corrosion susceptibility—and increase solid solution solubility of alloying elements, thus raising the potential of the matrix and possibly changing the composition of the passive film to an improved protective layer.

Application of the SMAT process alone has significant potential to improve the corrosion resistance of the substrate material and provide new avenues for exploring fundamental relationships between microstructure and corrosion response. However, it also has the capability to alter the surface chemistry of the substrate in addition to the surface morphology and microstructure through a direct mechanical (nonchemical) method. The desired surface coating results from incorporating material in powder form to be mechanically mixed with the substrate through the SMAT process. Mechanical alloying, as a solid-state mixing process, has the energy necessary to create nanostructured surfaces on both metals and ceramics and to mix nanocomposites. As an alternative to chemical anodizing, we hypothesized that SMAT of alumina powder stock onto an aluminum alloy or other alloy substrate can provide a robust, adherent, corrosion protection coating that avoids both the toxicity of traditional anodizing baths (e.g., chromate-based, strong acids) and the large amount of generated hazardous waste. As both the incorporation of new material (alumina) as a surface layer and the desired redistribution of precipitate phases (aluminum substrate) are not well captured in

the initial SMAT acronym, we devise a new process name: Surface Mechanical Alloying for Specialized Heterogeneity, or SMASH.

Results: Grain refinement of the substrate was achieved using steel media in both the AA2024 and AA5083 substrates. Additionally, the distribution and size of precipitate phases were altered. In AA2024 the precipitates were reduced in size, but that did not have an observable influence on the polarization behavior. However, the grain refinement in AA2024 led to an increase in exfoliation corrosion. The effect of the SMASH treatment on corrosion in AA5083 was far more positive. The chemical redistribution caused by the plastic deformation lowered the magnesium (Mg) content in the matrix such that the deleterious β phase precipitates are not expected to form. After sensitization heat treatments, no β phase was observed near the SMASH treated surface.

When using SMASH to produce an alumina surface layer from alumina powder, layers of 20–100 μm thick were formed on aluminum alloy substrates under a variety of processing routes—both alumina and steel impact media—and a variety of process times. Alumina media was more successful at producing a dense coating without cracking in the substrate.

Benefits: This limited scope program has shown the feasibility of the SMASH treatment to improve the corrosion response of AA5083. The mechanism for this improvement—reduction of Mg content into the depth of the substrate as a result of plastic deformation—is not one that has been observed before in other methods of severe plastic deformation applied to AA5083 and opens up new methods for improving sensitization behavior of Al–Mg alloys.

The SMASH process was successful in producing an alumina layer on aluminum alloy substrates through a mechanical mixing approach that uses only powder as input and discard (e.g., no acid baths as hazardous waste). However, the coatings have a range of particle distribution and are morphologically very different from traditional anodized coatings. Significant further testing is necessary to determine how this would affect adhesion and wear.

1. Introduction

Current surface treatments to impart desired surface chemistry and morphology on a metallic substrate, such as the anodizing of aluminum (Al) alloys, entail intensive multistep chemical processing systems that generate a significant amount of hazardous waste. The limited scope program seeks to understand and develop the fundamental principles of Surface Mechanical Attrition Treatment (SMAT) as related to surface grain size distribution and alloy composition so that surface characteristics of US Department of Defense (DOD) materials can be tuned for particular chemical, morphological, and mechanical properties without the need for chemical or electrochemical methods. The severe plastic deformation (SPD) and mechanical mixing inherent in the single-step SMAT process will be used to develop an optimized surface and subsurface macro- and microstructure such that adhesive and mechanical bonding, long-term durability, and corrosion resistance are enhanced.

The objective of this work is to explore the feasibility of SMAT to simultaneously improve the corrosion resistance of the substrate while imparting desired surface chemistry and morphology. This limited scope project has two aims: 1) quantify the ways in which a gradient microstructure achieved through a novel SPD method can enhance the corrosion resistance of a treated aluminum alloy substrate and 2) extend and develop this surface treatment to engender a surface alumina layer in single-step method without hazardous chemical processes.

In Task 1, the relationship between grain refinement and corrosion response is not currently well understood. The processing methods required impart metallurgical and morphological changes in addition to grain size that will also affect the corrosion response. The use of SMAT as a processing method enables deconvolution of some of the microstructure/corrosion relationship as the introduction of a grain size gradient helps efficiently quantify corrosion response based on specific microstructure. In Task 2, using the novel surface alloying treatment to create an alumina layer should result in different properties than an alumina surface generated through the chemical anodization process; for example, layer adhesion, porosity, and surface morphology. The SMAT surface alloying method should demonstrate improved adhesion to the substrate as it is a high-energy mechanical mixing process. We hypothesize that the resulting engineered surfaces will result in corrosion resistance and adhesive bonding, thereby enabling replacement of current hazardous chemical processes and improved material tolerance for extreme environments.

A successful project will demonstrate improvement in the substrate corrosion response through grain size and precipitate control of the treated surface/subsurface microstructure (Task 1) and show the viability of developing an aluminum oxide layer (Task 2) on AA2024 and AA5083 through the nonchemical process of SMAT. Inherent in both these tasks is the detailed characterization and quantification of corrosion response using accelerated corrosion, electrochemical, in situ electrochemical, and scanning probe methodologies. Both tasks will examine the impact of processing parameters on microstructure and corrosion response. These alloys were selected based on their importance in DOD applications and due to their potential to study the impact of SMAT on different types of corrosion behavior: In AA2024, corrosion initiates at intermetallic/matrix interfaces, whereas in AA5083 sensitization leading to intergranular corrosion is dominant.

2. Background

2.1 Strategic Environmental Research and Development Program (SERDP) Relevance

Commonly, Al anodizing is done in accordance with MIL-A-8625F *Anodic Coatings for Aluminum and Aluminum Alloys*.[1] In this specification, six types of anodizing are described. Two of these types rely on anodizing from chromic acid baths, and three types use sulfuric acid baths. Only one type of anodizing, type IC, is mentioned in the specification as a nonchromic acid alternative that can use a variety of organic acids. As awareness rises regarding the environmental dangers associated with the use of hexavalent chromium, the push for eliminating its use also rises, and although chromic acid alternatives exist, there are no known methods for creating an anodized layer on Al without the use of acids or electrochemical methods.

When formed electrochemically, properties such as corrosion or wear resistance vary with the type of anodizing bath: the thickness, uniformity, and porosity of the anodized layer; the postanodization sealer used; and the underlying alloy on which the anodized layer was formed. For instance, the anodized layers from chromic acid anodizing baths are typically thinner and softer than those formed from sulfuric acid baths, and although sulfuric baths can be used to make thin coatings, they are used mostly for thick “hard coat” layers formed at low temperatures.

The properties of the anodic layer depend both on anodization parameter space and substrate microstructure/morphology. For example, NASA has reported delamination of the black anodic coatings on 2XXX- and 7XXX-series aluminum alloys using the standard Type II process described in MIL-A-8625 due to

heterogeneous alloy phase composition in the substrate. Therefore, it is recommended that Type III anodization is used for 2XXX- and 7XXX-series aluminum alloys expected to experience thermal cycling.[2] This recommendation adds to the cost of anodization in that Type III hard-coat anodizing requires more energy to lower the bath temperatures to near the freezing point of the bath (~0 °C) and to oxidize at the requisite higher current densities.

Developing an environmentally friendly technology to impart an inorganic oxide into the surface of a metal without the use of acids could both reduce the constraints on attainable properties imparted by traditional anodization methods and significantly mitigate hazardous waste and worker exposure concerns with the current multistep chemical processes.

2.2 Corrosion Mechanisms

The two predominant corrosion mechanisms of the AAs selected are described in the following, briefly summarizing some background literature describing the use of various methods to alter the microstructure of the alloy that motivate the attempt to improve the corrosion response of the substrate via SMAT.

2.2.1 AA2024: Micro-galvanic

Galvanic corrosion refers to the interaction of two materials with different electrochemical properties in contact, wherein the difference in electrode potential between the two metals in aqueous environments acts as a driving force for corrosion of the less noble metal. For example, a more active metal is more likely to behave as an anode and experience a faster corrosion rate than that which would be associated with the anode alone. Conversely, the cathode experiences a slower corrosion rate, if at all, in the galvanic couple than in isolation. If this process continues, it is possible the cathodic phase will break away from the anodic phase, thus eliminating the galvanic couple. The corrosion rate of the cathodic phase will then increase to that of the self-corrosion rate and in the process disperse micro- and nano-sized particles into the solution, which then migrate to the surface and repeat the cycle of galvanic corrosion again. Many studies have shown that AA2024 is an exemplary system in which this corrosion mechanism is active.[3] Thus AA2024 is ideal for examining how the corrosion rate is influenced by the surface treatment (e.g., anodization, organic coating, laser processing, and peening).

In AA2024, as many as nine second phases exist in contrast to the solid solution matrix, and are a combination of cathodic (Al/copper [Cu]/iron [Fe]/manganese [Mn] and Al/Cu/Fe) and anodic (S phase) phases with respect to the matrix, which in turn contributes to multiple forms of corrosion.[3–5] The predominant phase,

however, is the S phase (Al_2CuMg).[6] Galvanic corrosion in AA2024 is reported to occur over a wide range of solution electrolyte and pH,[7] further highlighting the pervasive problem.

2.2.2 AA5083: Sensitization

AA5083 is generally considered to have excellent corrosion resistance compared with other aluminum alloys. However, at relatively low temperatures (~50 °C), which are possible in the service life of DOD applications, sensitization, a process by which Al_3Mg_2 (β phase) forms at grain boundaries, occurs. This β phase is more active than the bulk material and preferentially dissolves intra-granularly in corrosive environments, thereby resulting in potentially catastrophic and unexpected failure of the alloy.

To combat this problem, stabilization efforts usually entail heat treatments that encourage preferential precipitation of β phase away from grain boundaries at temperatures just under the solutionizing temperature; or, when β phase already exists on boundaries, to coarsen the precipitates to reduce the fractional grain boundary coverage.[8] It may be possible to replicate these efforts through the grain refinement process via SMAT, avoiding costly and time-consuming heat treatments.

As grain refinement increases, the grain boundary area increases significantly while the chemical composition remains the same; therefore, the fractional grain boundary coverage by either solute or precipitates has the potential to be greatly reduced.[9] In Kus et al.,[10] where nanocrystalline alloys were made from spray atomized AA5083, the Nitric Acid Mass Loss Test (NAMLT) showed that the nanocrystalline samples were less susceptible to intergranular corrosion, falling in the range of resistant materials. For clarity, NAMLT is used to assess the degree of sensitization (DOS) of alloys containing this soluble β phase. Alloys with a DOS of less than 15 mg/cm^2 are not considered to be sensitizable, whereas a general agreement exists that those with a DOS of 25 mg/cm^2 or greater are susceptible.[8]

Additionally, the processing aspect of grain refinement through SMAT/SPD offers significant opportunities for grain boundary and texture engineering, which will affect β phase precipitation during sensitization. Texture control in a small-scale sputtering process showed reduced β phase precipitation based on orientation distribution,[11] and numerous studies have highlighted the importance of grain boundary type to β phase nucleation, growth, and grain boundary coverage[12–14] (e.g., the β phase preferentially nucleates at low-angle grain boundaries, but high-angle grain boundaries have ~3 times larger precipitates[12]). Moreover, the high degree of dislocation density in the interior of grains typical of SMAT/SPD

processed materials provides additional sites for precipitation of intragranular rather than intergranular β phase.

A very recent result showed that below a certain threshold of grain size (where the size of the β phase and the grains were similar), grain size reduction introduced an additional factor in lowering sensitization past the effect of misorientation.[9] The gradient grain size produced via SMAT can be below this threshold at the surface,[15,16] potentially further improving sensitization behavior.

2.3 Alteration of Alloy Microstructure

It is clear that the grain size can indirectly contribute to the corrosion response by affecting other related factors, such as the nature of β phase precipitation as previously described. However, it can also in and of itself influence corrosion. The SMAT process induces grain refinement at the surface, but whether this will be beneficial or detrimental is not well established, with conflicting reports across various materials and corrosion environments. Reviews on the subject even indicate discrepancies within the same alloy system,[17–19] with an example being pure Al. Some reported a decrease in corrosion rate with grain reduction, while others reported a degradation in the passive film's ability to protect the underlying material, still others reporting there was little to no effect on pitting or repassivation.[20–23]

A reduction in grain size has recently shown good potential for improvement in various types of corrosion response (including reduced corrosion rate,[18,20] pitting potential,[24,25] stress corrosion cracking,[26] and intergranular corrosion susceptibility)[9] in addition to the more thoroughly studied gains in mechanical properties. However, unlike the generally direct relationship between grain size and mechanical strength, the correlation between grain size and corrosion is not straightforward and must be discussed in terms of the processing history. For example, the same grain size in the same alloy obtained through different processing methods have been shown to exhibit differences in both thermodynamic (corrosion potential) and kinetic (corrosion current) behavior.[9,27] Additionally, both the processing routes to achieve significant grain size reduction and the newly increased grain-boundary volume fraction will have implications for the precipitate phases that often dictate corrosion response.

Grain refinement, especially to the nanoscale, requires a far-from-equilibrium processing method. Most commonly this is a form of SPD such as mechanical alloying (which uses repeated high-energy impact of shot to impart plastic deformation) or Equal Channel Angular Extrusion (ECAE), in which a material undergoes several passes through a channel with a 90° bend to impart large strains.

In general, grain refinement occurs through deformation-induced dislocation generation, which breaks up both existing grain boundaries and chemical phases on the path to generating new dislocation networks that form new, finer-spaced grain boundaries. SPD processes therefore not only change the grain size, but also the character of the grain boundaries (e.g., misorientation, texture, and high angle vs. low angle) and the distribution of solute (whether through breakup of phases or increased solid solubility).

For example, in AA2024, corrosion response is mainly driven by the S phase (Al_2CuMg) precipitate/matrix interface. Susceptibility to intergranular corrosion decreased as a result of ECAE processing, as the dominant corrosion mode shifted from intergranular corrosion to pitting as the S phase was redistributed from the grain boundaries to the matrix.[28] Other plastic deformation processes that significantly altered the size and distribution of intermetallic phases in 2024 were friction stir welding[29] and ultrasonic shot peening,[30] with varying results to the corrosion response. Conversely, in AA5083, where the deleterious precipitates are not present in the initial material but instead form during service, the high-dislocation densities resulting from plastic deformation processes provided enhanced pathways for diffusion and subsequent higher growth rate of β phase leading to increased susceptibility to sensitization.[31]

It is clear that generalizations cannot be made about the effects of microstructural alteration via plastic deformation processes without investigating the particular process in question.

2.4 Surface Deformation

SMAT is a relatively unexplored severe surface deformation process that produces a nanocrystalline/ultra-fine-grain layer of varying depth and gradient, as shown in the treated pure nickel plate in Fig. 1.[16] The SMAT process employs repeated high-energy impact of spherical shot on the surface to cause plastic deformation that results in surface grain refinement similar to other surface modification processes, such as shot peening. However, SMAT can significantly increase the kinetic energy of the media over that of shot peening, imparting an increase in surface grain refinement and work-hardened depth[32] as well as larger residual compressive stresses.[33] These attributes have initially been explored in the context of improved mechanical properties; however, as described, they also have the potential to impart significant improvements to corrosion resistance. In this work we have devised a new acronym, Surface Mechanical Alloying for Specialized Heterogeneity, or SMASH, to replace SMAT, as we are not attriting material but adding it to form a surface layer in Task 2. Additionally, the desired modification

of alloy chemistry of the substrate (Task 1), through the redistribution of precipitate phases, is not well captured in the initial acronym.

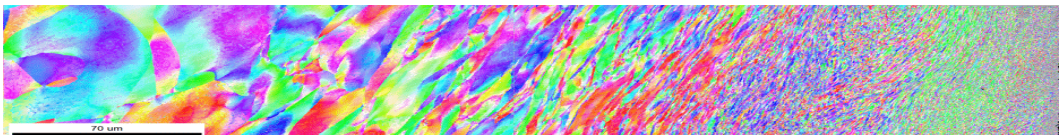

Fig. 1 Example grain size gradient microstructure produced using the SMASH process on pure nickel substrate at CCDC Army Research Laboratory. Impacted surface is on the right-hand side.

3. Materials and Methods

3.1 SMASH Process

A SPEX SamplePrep 8000M Mixer/Mill was used for the SMASH treatments. The apparatus consists of a vial within which impact media (shot) is placed; the substrate to be treated replaces the lid of the vial. The plates are discs nominally 2 inches in diameter. In this work, two different process media were used: steel and alumina. For the steel media SMASH treatments, a tool steel (52100) vial and stainless steel (44 °C) shot were used. Based on the author's previous work using steel media,[16,34] 50 g of 8-mm-diameter shot was used. Additionally, before treatment of the substrates, 0.5 g of Al powder was run in the mill to coat the shot and vial with the goal of reducing pickup contamination from the steel vial and shot during SMASH treatment.[33]

For the alumina media SMASH treatments, an alumina vial and alumina shot were used. The alumina shot was 3/16 inch in diameter. Due to the significantly lower density of the alumina shot vis à vis the steel shot, only 10 g of alumina shot was used to approximately maintain the volume ratio of shot-to-vial chamber area. This allows free travel of the shot around the vial to subsequently interact with the substrate rather than mostly interacting with other shot. For the surface alloying experiments, α-alumina powder of one of two sizes (+120 and –325 mesh; coarse and fine, respectively) was added to the vial before the SMASH treatment.

3.2 Microstructural Characterization

Specimens were cross sectioned and prepared with standard metallographic procedures down to 0.05-µm diamond polish. Polished samples were etched with Kroll's reagent. Optical microscopy was performed on an Olympus LEXT OLS3100/3000 confocal microscope, and scanning electron microscopy (SEM), electron dispersive X-ray spectroscopy (EDS), and electron backscatter diffraction

(EBSD) were performed on a FEI NanoSEM 600. EDS was used to characterize the chemical distribution and performed with an EDAX Octane Elite Super system. The EDS maps were thresholded based on matrix chemical composition to determine the precipitate size and area fraction. Scans were done at four different areas on each specimen to garner at least 100 precipitates. EBSD was used to characterize grain size and grain boundary distribution.

3.3 Corrosion

3.3.1 Open Circuit Potential

Prior to polarization experiments, the open circuit potential (OCP) was monitored for up to 18 h in 0.6-M sodium chloride (NaCl) (aqueous). An overpotential was applied only after the OCP was stable.

3.3.2 Potentiodynamic Polarization

Electrochemical measurements were made in a flat cell with a working electrode area of 1 cm^2. The aluminum alloy sample was the working electrode, a platinum-coated titanium wire mesh was used as a counter electrode, and a saturated calomel electrode (SCE) served as a reference for the three electrode configuration. Samples were polarized at a rate of 10 mV/s from –0.5 to 1.5 V of the OCP.

3.3.3 Exfoliation

Exfoliation corrosion susceptibility was evaluated using ASTM G34.[35] The specimens were immersed in an aqueous solution of NaCl (4.0 M), KNO_3 (0.5 M), and HNO_3 (0.1 M). Samples were approximately 1 × 1 × 0.5 cm, and the edges and back were masked with Kapton tape so that only the SMASH surface (or as-received surface) was exposed to the solution. Observation intervals were 6, 24, 48, and 96 h for as-received AA2024 and 96 h for SMASH AA2024.

3.3.4 Sensitization

AA5083 H131 samples were sensitized to promote β phase (Al_3Mg_2) formation at the grain boundaries. Sensitization was accomplished by holding samples at 125 °C for 28 days in an oven filled with ambient atmosphere. AA5083 samples were also sensitized at 125 °C for intermediate times of 7 and 14 days.

3.4 Hardness

Vickers hardness measurements were performed with a 25-g load and 10-s dwell time with a Wilson Tukon 1202 hardness tester. Indents were placed 25 μm from the surface with a uniform spacing of 25 μm up to a depth of 500 μm into the surface or until the hardness plateaued. A total of five indents were averaged at each depth. Nanoindentation was conducted with a Keysight Technologies (formerly Agilent) Nano Indenter G200 instrument on both the sensitized and unsensitized baseline and SMASH AA5083 samples. A 10 × 10 array of indents was generated, with the first row of indents positioned 25 μm from the surface and the last row at a distance of 975 μm from the surface. Thus 10 indents were averaged every 50 μm from the surface. Indents were displaced to 2000 nm.

4. Results and Discussion

While the corrosion response of both alloys is determined by the electrochemical heterogeneity introduced by precipitate phases, the first example is controlled by existing precipitates; the second, the ensuing formation of precipitates during service conditions. As such, we will examine the effect of the SMASH process on the microstructure of these two types of alloys for a thorough fundamental understanding of the effects of process parameters on the substrate and its subsequent corrosion response. Section 4.1 describes the work on AA2024 and Section 4.2 on AA5083. Next the SMASH process is used to produce a surface layer of alumina on the aluminum alloy substrates through mechanical, *not* chemical, means. These results are described in Section 4.3

4.1 AA2024 Substrate Microstructure Development

The hypothesis for improving the corrosion response of AA2024 is that fragmentation of the precipitates will lessen the accelerating corrosion effects of micro-galvanic couples. The effect of grain refinement on corrosion response has many possible outcomes.

4.1.1 Microstructure

The baseline AA2024 has elongated grains with widths of 50–100 μm and lengths in the millimeters. A representative microstructure can be seen on the left-hand side of Fig. 2. The microstructures of the AA2024 substrate subjected to the SMASH treatment using various times and media are on the right-hand side of Fig. 2; steel media are on the top row and alumina media on the bottom row. The scale bar is the same for all images and the treated surface is on the top of the image (black region is the sample mount). Only the AA2024 treated with steel media showed

significant grain refinement, extending about 200 µm into the substrate. Increasing the treatment time, from 0.5 to 1 h, did not significantly increase the depth of this grain refinement. A reduction in the surface grain size is not observed in the samples using alumina media for the SMASH treatment (Fig. 2, bottom row). The grain size is one aspect that may influence the corrosion response of the aluminum substrate, but the chemistry of the surface is imperative. EDS scans were next performed to quantify the chemical distribution as a function of SMASH treatments.

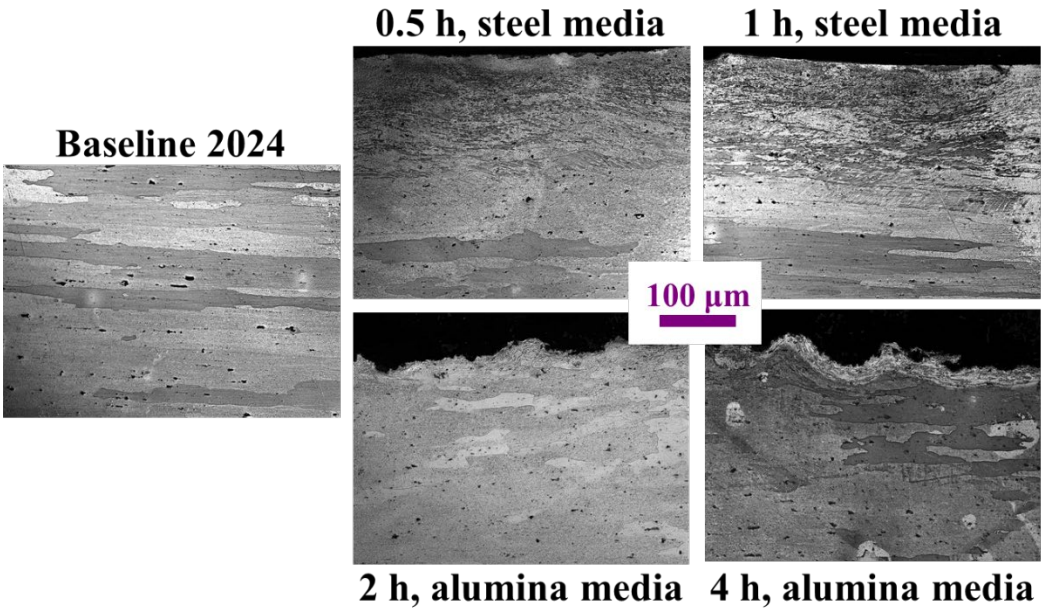

Fig. 2 Optical micrographs of baseline AA2024, SMASH AA2024 with steel media (top row), 0.5- and 1-h treatments; (bottom row) alumina media, 2- and 4-h treatments

AA2024 has many intermetallic phases[6] that can create micro-galvanic couples with the matrix, and all contain Cu in some measure. Therefore, the Cu EDS map is presented in this report and used to enumerate the intermetallic phases. Figure 3, left-hand column shows the EDS map of Cu in a) the baseline AA2024, b) the 0.5-h steel media, and c) the 1-h steel media. From these maps the average precipitate diameter was calculated for the region of the substrate starting at the surface and continuing to a depth of 25 µm, and the results are presented in Table 1. The initial average diameter of a precipitate was 7.94 µm, and the average area fraction was 2.95%, in line with other observations for this alloy and temper (Boag et al.[6] and references therein). After 0.5 h of SMASH with steel media, the precipitate size has dropped to 3.32 µm and after 1 h, the average diameter is now 1.82 µm. The area fraction has not changed significantly.

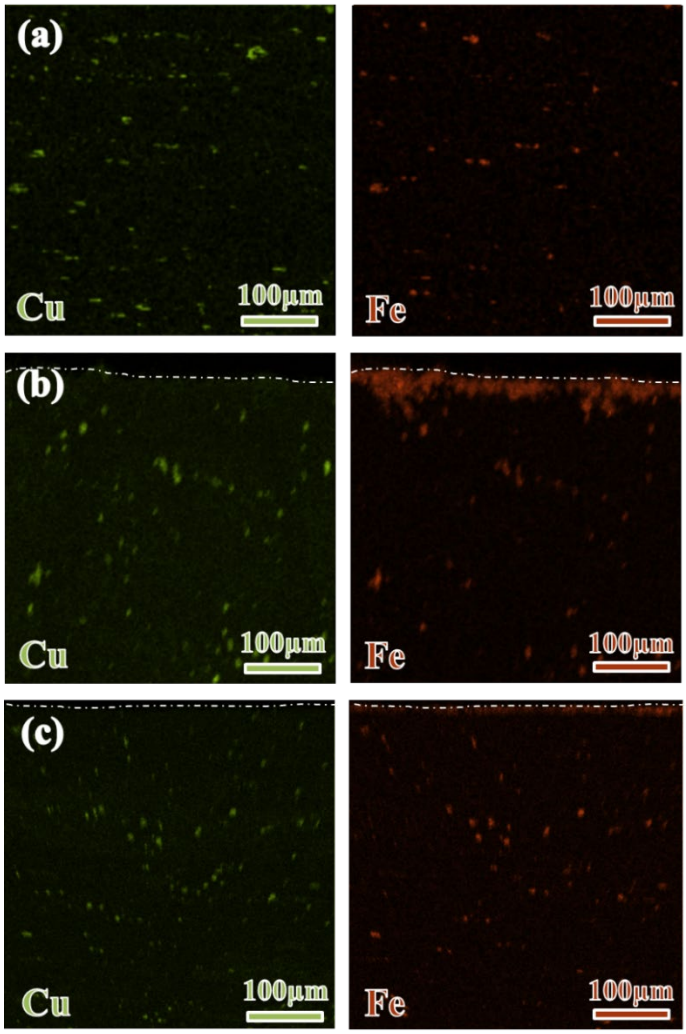

Fig. 3 EDS maps of Cu and Fe for a) baseline AA2024, b) SMASH AA2024 0.5 h, steel media, and c) SMASH 1 h, steel media. Treated surface is indicated by dashed white line.

Table 1 Microstructural quantification for SMASH AA2024

Media	Precipitate diameter	Cu area fraction	Fe area fraction
Baseline AA2024	7.94 µm (±3.77 µm)	2.95%	1.21%
0.5 h, steel	3.32 µm (±1.71 µm)	2.62%	30.9%
1 h, steel	1.82 µm (±1.59 µm)	2.86%	5.98%

The EDS maps of the SMASH treated AA2024 using steel media, Fig. 3b and c on the right-hand column, show significant contamination from the steel media, with almost 30 times the iron content as the baseline in the 0.5 h sample and 6 times in the 1-h sample. While the method of precoating the treatment vial and media with the substrate (in this case Al) powder to combat pickup contamination has been

successful in other systems,[34] it is clear that it was ineffective in the case of AA2024. Thus, we examine the use of alumina shot and alumina vial on the surface chemistry of the treated substrate. Figure 4 shows EDS maps for SMASH-treated 2024 alloys using alumina media with a 4-h treatment time. Unsurprisingly, in both the 2- and 4-h treatments, considerable amounts of alumina were observed on the surface. There was no congregation of Fe on the surface as was seen in the samples impacted with steel media.

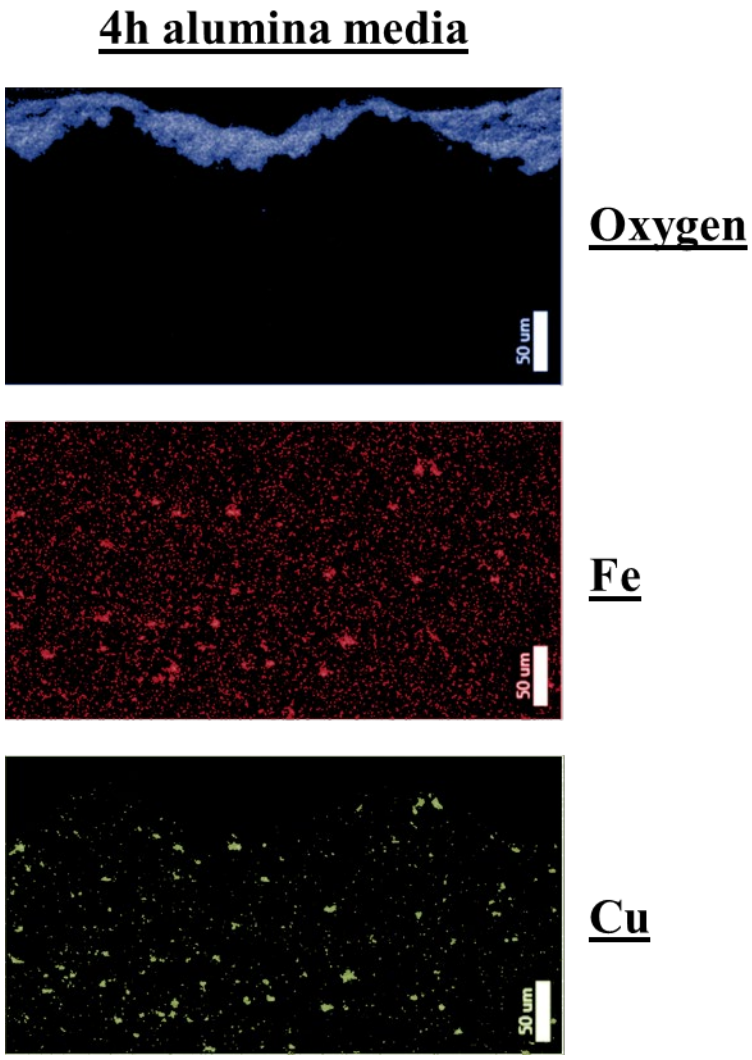

Fig. 4 EDS scans of AA2024 4-h SMASH with alumina media. Treated surface is at the top of each image.

4.1.2 Hardness

Based on the AA2024 substrate microstructures reported in Section 4.1.1, only those specimens with visible grain refinement—the 0.5- and 1-h SMASH with steel shot media—are evaluated for microhardness. The results are shown in Fig. 5, with

hardness as a function of depth into the substrate and compared with the hardness of the baseline 2024 alloy (green dashed line). Both the 0.5- and 1-h SMASH treatments with steel media show an increase in hardness in approximately the top 200 μm of the substrate, in line with the observed grain refinement shown in the top two images of Fig. 2. The hardness value measured closest to the surface, at a centerline of 25 μm, is somewhat higher for the 0.5- than for the 1-h treatment. Considering the differences in Fe contamination between the two samples, wherein the 0.5-h treatment exhibited approximately five times that of the 1-h treatment, it is likely a result of the higher hardness of both the tool steel (contamination from vial material) or stainless steel (contamination from shot material) used as the media. While the Fe contamination does not generally extend 25 μm deep into the substrate, this value is where the measurement is centered. The width of an indent is around 15 μm, reaching into the Fe-contaminated region. Hardness values from the next data point (centered at 50 μm), and onward, should reflect the grain refinement only and are comparable with literature reports[36,37] in which plastic deformation is performed at cryogenic temperatures to achieve a reduction in grain size. Contrastingly, when a high-temperature deformation process, friction stir welding,[29] is used, the reduction in grain size was *not* accompanied by an increase in hardness. The high temperature impacts the fine-scale precipitates, which are providing the main strengthening mechanism for the aluminum alloy. The SMASH process imparts a slight temperature rise above room temperature (at which it is performed). However, based on the hardness results of Fig. 5 and the expected increase in hardness with decrease in grain size, it appears the fine-scale strengthening precipitates have not been negatively impacted, at least enough to offset the improvement in hardness wrought by the smaller grain size.

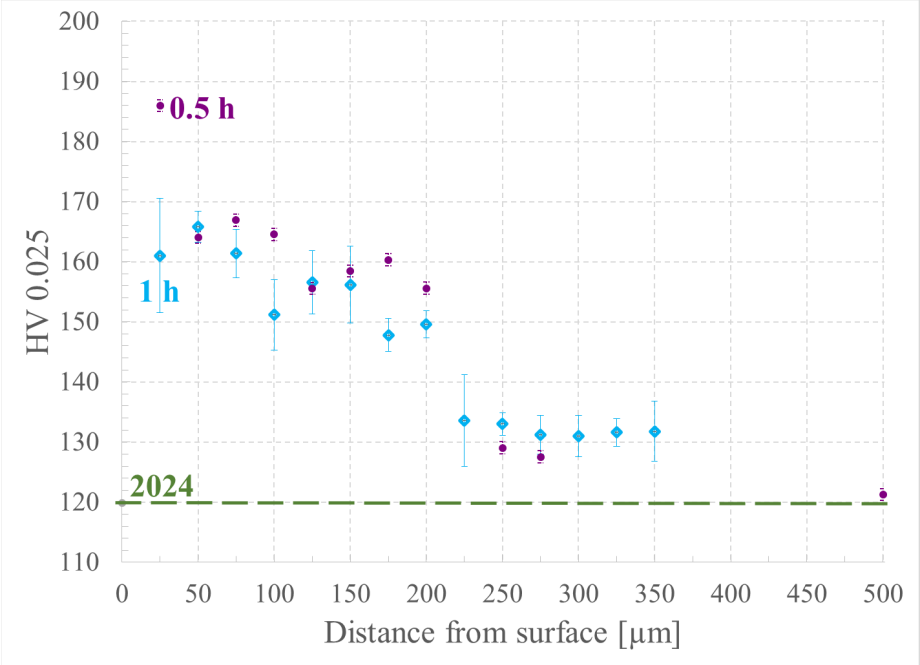

Fig. 5 Microhardness of the AA2024 SMASH treated with steel media for 0.5 h (purple circles) and 1 h (aqua diamonds) as a function of depth into the substrate. Baseline AA2024 hardness is indicated by green dashed line.

4.1.3 Corrosion

Given the significant Fe contamination on the surface, it was expected that the OCP would shift from the baseline AA2024; however, it has remained in the standard range for the aluminum alloy, around 600 mV versus SCE, as can be seen in Table 2. This is also the range for low-carbon steels. Interestingly, the Fe contamination appears then to be more from the tool steel vial than from the stainless steel shot. This is confirmed by EDS observations of the chromium (Cr) content in the Fe-contaminated region. There is very little observed Cr, as befits the content of the tool steel (~1.5 wt%) as compared with the stainless (~13 wt%). In the alumina media SMASH samples, the cathodic kinetics increased, perhaps due to additional defects introduced into the native oxide and surface layer (Fig. 6, right-hand side).

Table 2 Selected corrosion data for AA2024

Media	OCP (vs. SCE)	Pitting potential (vs. OCP)
Baseline AA2024	–600±4 mV	…
0.5 h, steel	–614±2 mV	541 mV
1 h, steel	–608±5 mV	522 mV

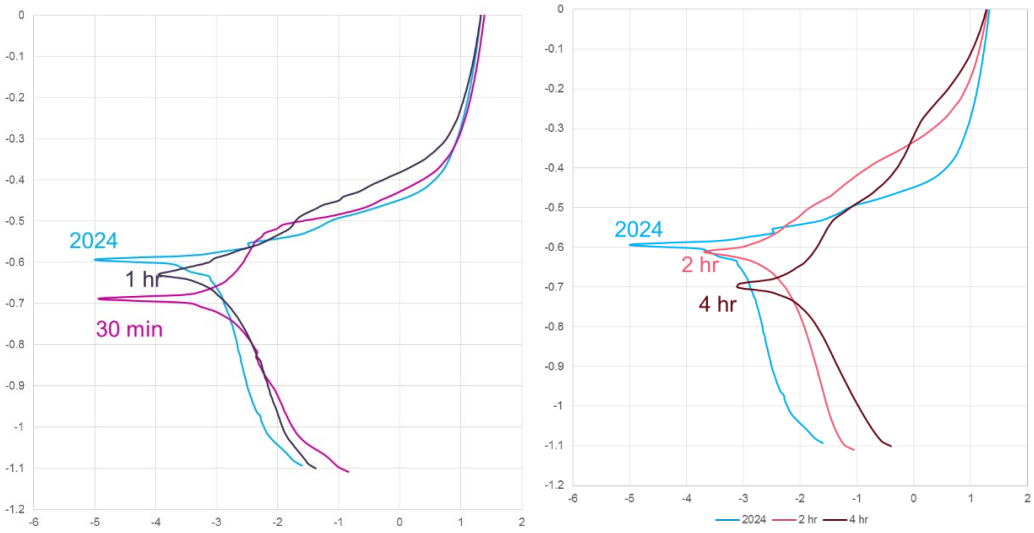

Fig. 6 Potentiodynamic polarization curves of AA2024 samples: (left) steel media and (right) alumina media

The results of exfoliation corrosion test showed that grain refinement negatively impacted the corrosion response in AA2024. Example SEM images are shown in Fig. 7, with the baseline AA2024 on the left and SMASH treated (1-h steel media) on the right. The SMASH-treated AA2024 has lost from 100 to 250 µm of material from the surface after 96 h of immersion, whereas the baseline AA2024 has not lost an appreciable amount after the same time interval. The material loss in the SMASH sample is approximately the same dimension of the depth of grain refinement into the substrate. It is likely that the high density of grain boundaries in this region provided pathways to accelerate intergranular corrosion and material loss as compared with the baseline material.

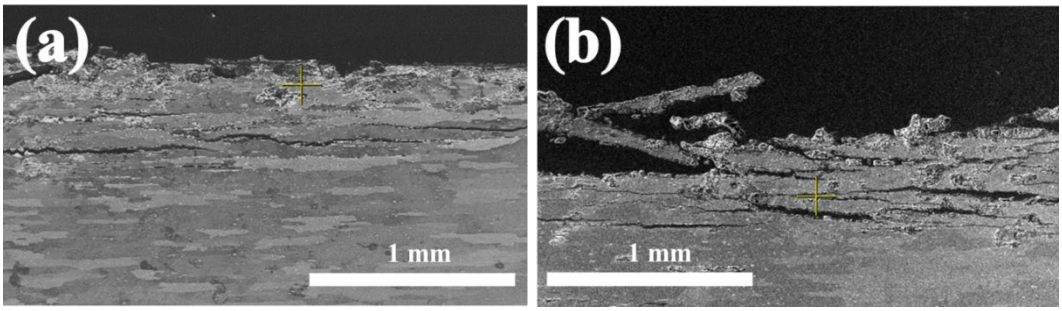

Fig. 7 SEM images of a) baseline AA2024 and b) SMASH AA2024 (1 h, steel media)

4.1.4 AA2024 Summary

- Grain size is reduced at the surface using steel media but not alumina media.

- Precipitate size is appreciably reduced by the SMASH treatment using steel media.
    - The lack of a significant corrosion response in the potentiodynamic polarization experiments was unexpected. These experiments used polarization parameters common throughout the literature for surveying large differences in polarization response. It is expected that subtle differences in pitting potential or dissolution kinetics can be teased out of the data by narrowing the polarization parameters to a smaller cathodic overpotential and slowing the scan rate.
- Significant surface contamination occurs for *both* steel and alumina media.
    - In the steel media, the contamination derives mostly from the vial, rather than the shot.
    - As the OCP for low-carbon steel (vial contamination) is similar to 2024, there is little change due to the SMASH treatment in steel media.
- Exfoliation corrosion response on the grain-refined substrate (steel media) was considerably inferior to that of the baseline, likely due to increased pathways for intergranular attack.

4.2 AA5083 Substrate Microstructure Development

The hypothesis for improving the corrosion response of AA5083 through the SMASH treatment is that the decrease of low-angle grain boundaries will reduce the preferential sites for β phase, and the grain refinement will increase grain boundary area to reduce total coverage of grain boundaries by β phase to lessen grain pullout.

4.2.1 Microstructure

A representative EBSD scan of the initial microstructure of AA5083 (plane of image in line with rolling direction) is shown in Fig. 8, left-hand side. The grains are around 50–100 μm in diameter. On the right-hand side of Fig. 8 is an EBSD scan near the surface of the SMASH-treated 5083 for 0.5 h using steel media (note that the scale bars in Fig. 8 are an order of magnitude different). There is considerable grain refinement to an average grain size of around 2 μm. This is an increase in grain boundary area of over 5000%. The distribution of misorientation of the grain boundaries in both the baseline and the SMASH-treated 5083 (0.5-h steel media) is in Fig. 9. Low-angle boundaries (those considered preferential nucleation sites for the deleterious β phase)[12] are generally deemed less than 15°

misorientation. The amount of these boundaries has been reduced from 34% in the baseline to 20% in the SMASH sample.

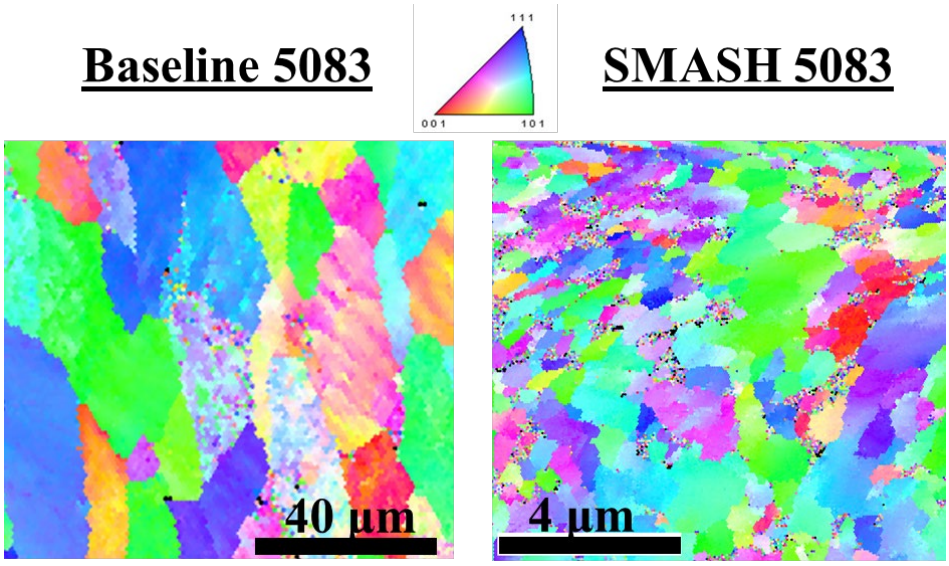

Fig. 8 EBSD scans of the baseline AA5083 and SMASH AA5083 (0.5 h, steel media) showing significant grain refinement

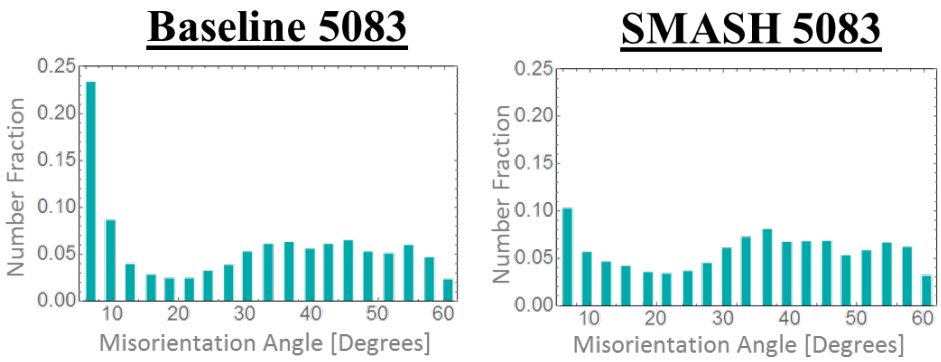

Fig. 9 Plots of number fraction of grain boundaries as a function of misorientation angle for the baseline AA5083 and the SMASH AA5083 (0.5 h, steel media)

Interestingly, the chemical distribution is also significantly altered near the surface of the substrate as indicated by the EDS scans in Fig. 10. The baseline 5083 microstructure is characterized by large Al_6Mn precipitates, clearly seen in the Mn EDS map and visible as the lightest gray phase in the SEM image. There is some solubility of Cr into this phase, visible in a few of the Al_6Mn precipitates in this region, as indicated by white arrows pointing to the darker clusters in the Cr EDS map, that are in the same location as the Mn EDS map and SEM image; the rest of the Cr is in solid solution in the Al matrix. There is also a small number of

Al–Mg precipitates, dark gray in the SEM image, and visible as dense spots in the Mg EDS map.

In the representative SEM image of the SMASH-treated AA5083 (0.5-h steel media), the top 50 µm have numerous light gray precipitates visible, smaller in scale than the baseline AA5083. As revealed by the EDS maps, these are *not* Al_6Mn, but instead an Al–Cr precipitate. Additionally, the amount of Mg present in this top 50 µm is less than that of the rest of the substrate. Presumably, the increased diffusion pathways through the severe plastic deformation process[38] enabled the dual migration of Mg and Cr in opposite directions. In an Al–Mg alloy, the extrusion process was found to "mechanically" sensitize the material, wherein the β phase formed on grain boundaries in the as-extruded specimen before any heat treatments.[39] Excitingly, in this SMASH treatment, the precipitate phase forming is *not* the β phase but an unusual (for this alloy) Al–Cr phase that has been found to be beneficial for corrosion response in other systems.[40] Additionally, the Mg content in the surface area has been reduced, limiting the available concentration necessary to form the β phase during the traditional sensitization process (low-temperature heat treatment).

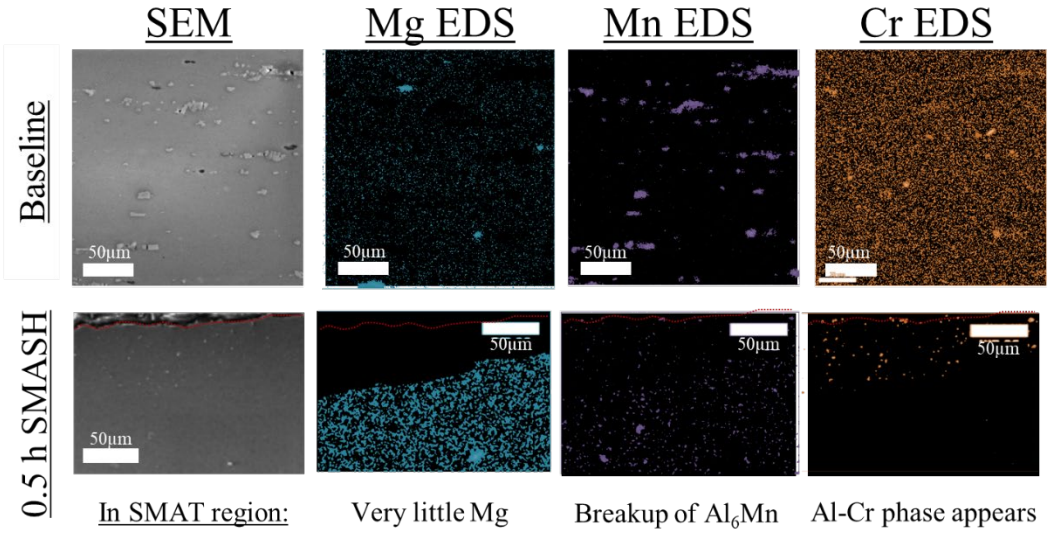

Fig. 10 (top row) SEM images and EDS maps of unsensitized baseline AA5083 and (bottom row) SMASH for 0.5 h, steel media. Treated surface is indicated by red dashed line.

4.2.3 Corrosion: Sensitization

The sensitization anneal (at 125 °C) was performed for 7, 14, and 28 days, and the microstructural evolution is presented in the following. Figure 11 depicts the microstructure of the baseline (top row) and the SMASH-treated (0.5-h steel media) 5083 substrates (bottom row). Similarly to the unsensitized baseline 5083 (Fig. 10, top row), the 28-day sensitized baseline 5083 is characterized by large Al_6Mn

precipitates of relatively the same size. Again, there is some solubility of Cr in this Al_6Mn phase, as evident by the regions pointed out by white arrows in the respective EDS maps. The SMASH 5083 continues to have a region about 50 µm thick from the surface with a chemical distribution distinct from the rest of the substrate. The surface region continues to be depleted in both Mg and the Al_6Mn phase as a result of diffusion away from the surface in favor of Cr precipitates. The unexpected Al–Cr precipitates are still present. Comparing the EDS maps of Cr from pre- and post-28-day sensitization treatment in Fig. 12, they are reduced in both size and area fraction coverage. The Al–Cr precipitates had an average size of 1.9 µm before and 0.8 µm after the 28-day sensitization anneal, and an area coverage of 3% and 1.5% respectively.

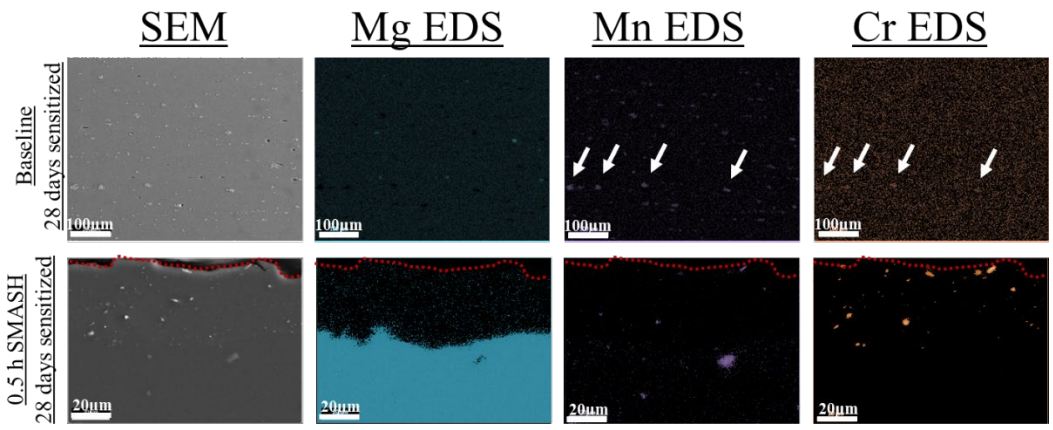

Fig. 11 (top row) SEM images and EDS maps for sensitized (28 days) baseline AA5083 and (bottom row) SMASH for 0.5 h, steel media. Red dashed line indicates the treated surface of the SMASH sample.

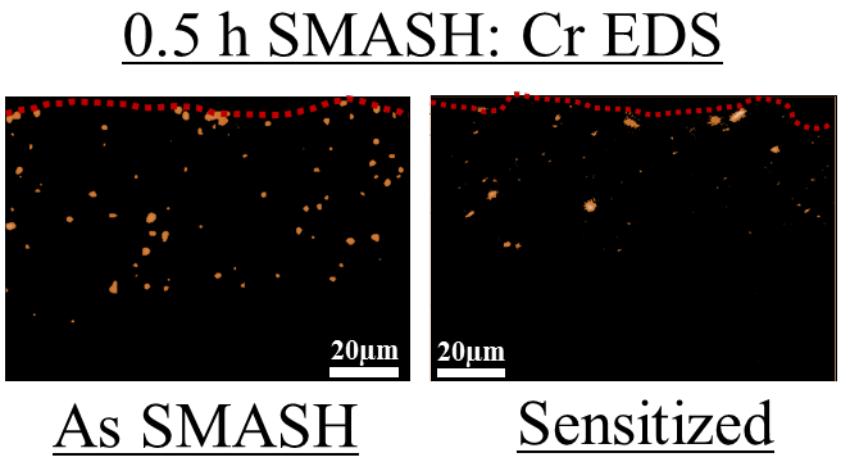

Fig. 12 (left) EDS map of Cr for SMASH AA5083 (0.5 h, steel media) before and (right) after sensitization treatment. Red dashed line indicates the treated surface.

The corrosion response of the sensitized and SMASH processed AA5083 (Fig. 13) showed a slight decrease in the pitting potential compared with the unsensitized AA5083 control. The corrosion current of the sensitized and SMASH + sensitized samples were nearly identical. Arguably there is a slight decrease in both anodic and cathodic kinetics at some potentials, but the magnitude of these differences is small.

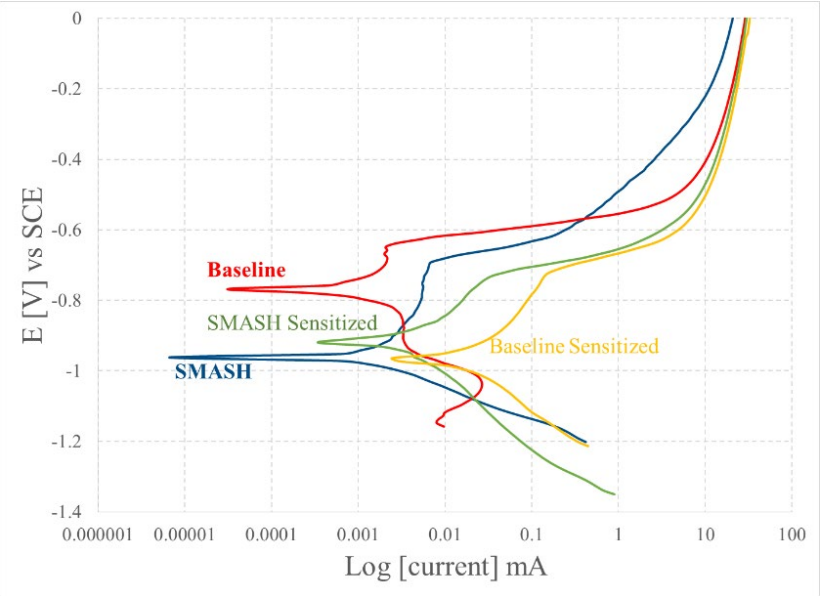

Fig. 13 Potentiodynamic polarization curves for the sensitized SMASH treated (0.5 h, steel media) AA5083 compared with baseline AA5083 alloy

Regarding sensitization, and the formation of β phase, the Mg concentration of the depleted region is now less than the threshold for β phase formation to occur (<3%). Correspondingly, Transmission Electron Microscopy analysis saw no β phase in the surface region of the SMASH AA5083 even after 28 days of heat treatment. Instead of improving sensitization response via grain refinement or grain boundary engineering, the chemical redistribution from plastic deformation actually prevented β phase formation.

4.2.2 Hardness

Nanoindentation is used here for its considerably smaller indent size rather than microhardness (as in the AA2024) due to the interesting chemical distribution and stark delineation in precipitates around a depth of 50 μm (Figs. 10 and 11). The strength was determined as a function of depth into the substrate surface for the SMASH-treated 5083 for 0.5-h steel media. Data for the unsensitized and sensitized (7, 14, and 28 days) conditions are presented in Figs. 14–17. The blue data points represent hardness values of the SMASH samples, and the bold dashed orange line

represents the average hardness of the corresponding baseline 5083 sample, with the two thinner dashed lines representing the error as indicated by standard deviation.

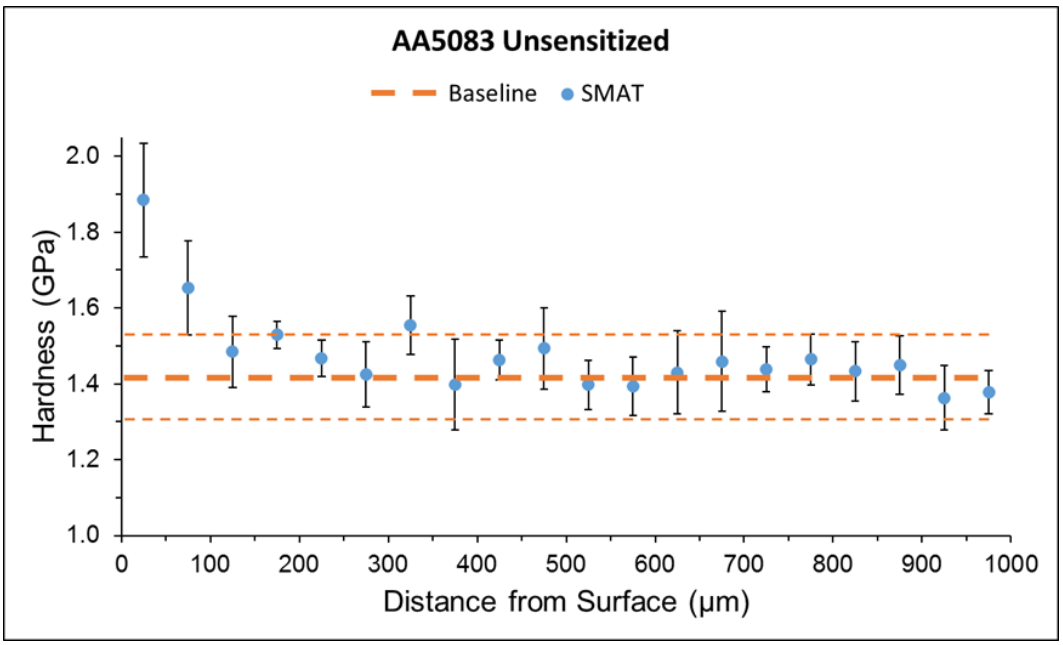

Fig. 14 Hardness as measured by nanoindentation for baseline AA5083 and SMASH AA5083 (0.5 h, steel media)

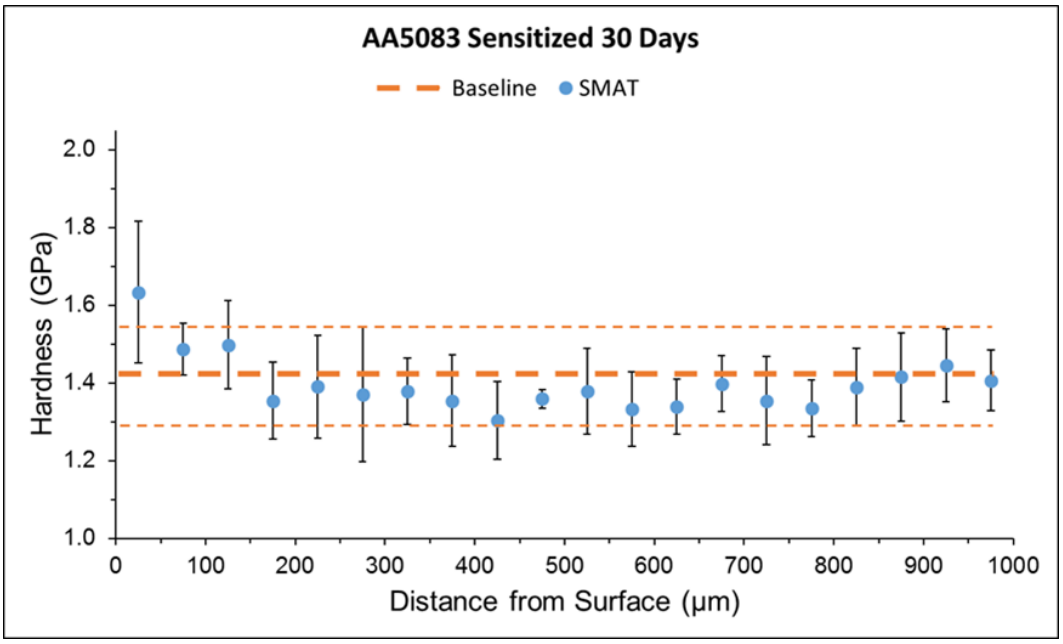

Fig. 15 Hardness as measured by nanoindentation for sensitized (28 days) baseline AA5083 and SMASH AA5083 (0.5 h, steel media)

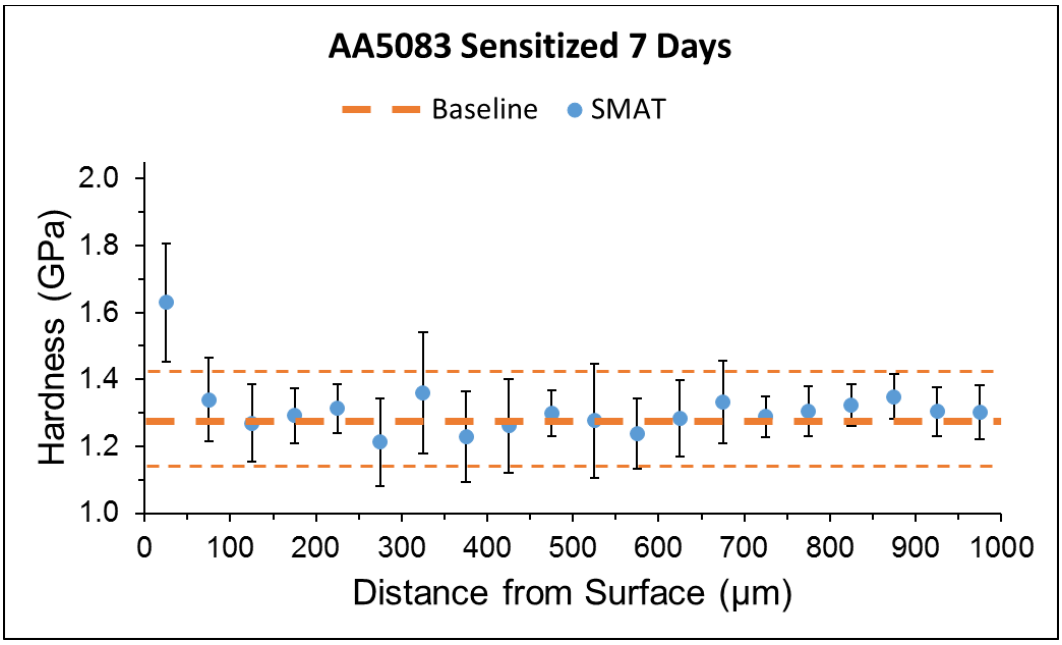

Fig. 16 Hardness as measured by nanoindentation for sensitized (7 days) baseline AA5083 and SMASH AA5083 (0.5 h, steel media)

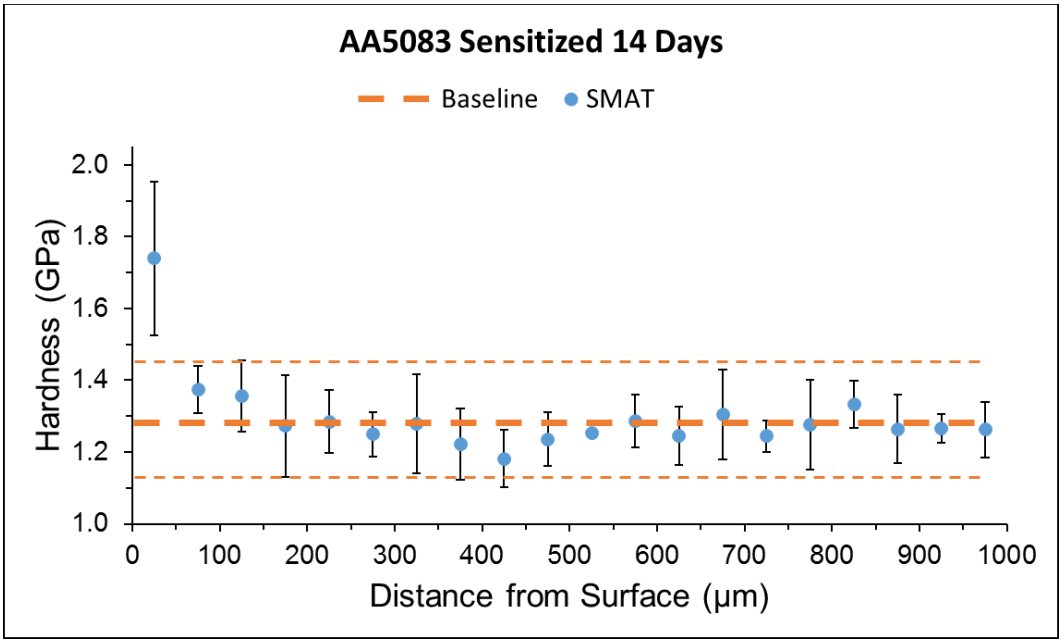

Fig. 17 Hardness as measured by nanoindentation for sensitized (14 days) baseline AA5083 and SMASH AA5083 (0.5 h, steel media)

For the unsensitized sample, the hardness increases as much as 0.5 GPa in approximately the top 100 μm of the substrate after the SMASH process. It is likely that the hardness at the very surface is even higher since indents were measured

starting at 25 μm from the surface to eliminate effects of the sample mount. This region of improved hardness exceeds that which underwent a chemical change.

The hardness of the sensitized SMASH samples decrease compared to the unsensitized SMASH sample to the point where its error is within the range of the baseline error. The SMASH hardness also reaches the baseline value faster (i.e., over a shorter distance: 50 vs. 100 μm from the surface) than did the unsensitized SMASH hardness. It is likely that an increase in grain size after 28-day sensitization is what drove the decrease in hardness compared with unsensitized SMASH.

4.2.4 AA5083 Summary

- Both grain size and low-angle boundaries were reduced by a SMASH treatment of 0.5 h with steel media.
- Hardness was increased for the top approximately 100 μm of the substrate.
- The chemical distribution in the top approximately 50 μm of the substrate surface was significantly impacted by the SMASH (0.5-h steel) treatment.
    - An unusual Al–Cr phase was present.
    - The Al_6Mn was fragmented.
    - There was a depletion of Mg in the matrix.
- Sensitization anneal was performed for intervals of 7, 14, and 28 days.
    - The top approximately 50 μm of the SMASH (0.5-h steel) substrate continued to present depletion in Mg and Al_6Mn and the unusual Al–Cr phase.
    - Depletion in Mg was such that the concentration was too low to form β phase.

4.3 Alumina Surface Alloying

The SMASH process was next investigated as a method to induce a surface layer of alumina onto the aluminum alloy substrates. Alumina powder was introduced into the SMASH process vial in a mechanical approach that has essentially no process waste other than unincorporated powder that can be reused.

4.3.1 Alumina Powder Size

Two sizes of α-alumina powder were used in the surface alloying task: coarse (+120 mesh) and fine (–325 mesh). Figure 18 shows large-scale SEM images of the surface layers produced by using 1 g of the coarse (top) and fine (bottom) alumina powders on AA5083 substrate with the same SMASH treatment (0.5-h steel media). The alumina layer is highlighted by the purple arrows. The surface layer produced by the fine powder is significantly thicker and has more-consistent coverage of the entire treated surface. In the coarse image, several areas with no or very little alumina coating can be seen. More significantly, a closer look at the interface shows many cracks in the substrate layer emanating from the interface (Fig. 19). Additionally, there are many areas where it appears that a segment of alumina layer was present and then was detached from the surface at some point during the SMASH treatment (left-hand side of Fig. 19). Given these results, the fine powder (–325 mesh) was used going forward.

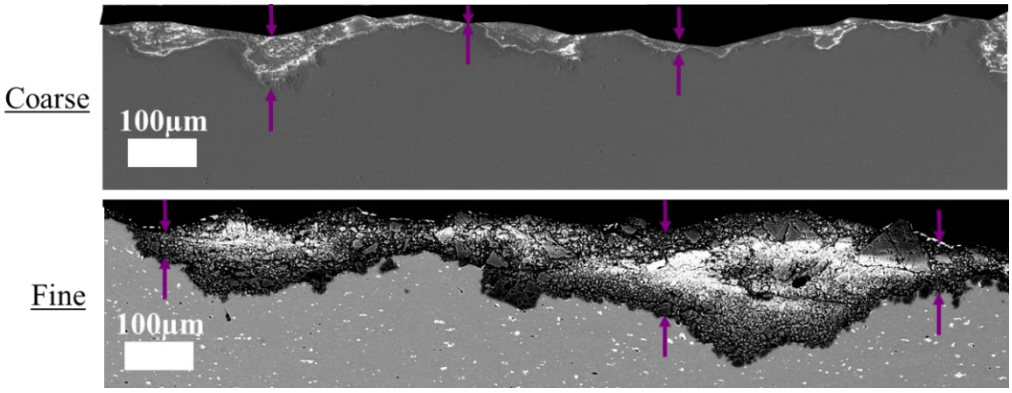

Fig. 18 SEM images of SMASH of 1 g of alumina powder with steel media for 0.5 h: (top) coarse (+120 mesh) and (bottom) fine (–325 mesh). Sample mount material is blacked out for clarity. Purple arrows indicate dimensions of the alumina layer.

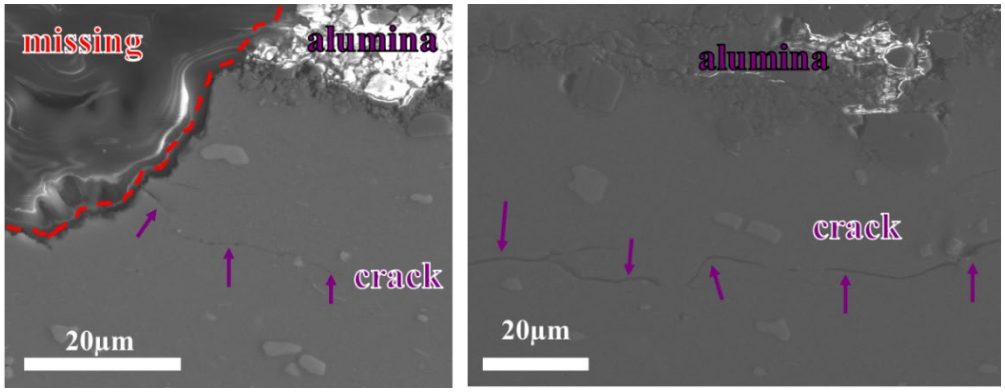

Fig. 19 SEM images of SMASH (0.5 h, steel media) with coarse (+120 mesh) powder. (left) Image highlights the removal of sections of the alumina layer during the process. Both images highlight the significant cracking observed emanating from the alumina/substrate interface.

4.3.2 Media

The same amount of fine (–325 mesh) alumina powder (1 g) was incorporated into the SMASH process for four processing conditions, two time intervals each for steel media and alumina media. Based on the significantly larger impact on the substrate that was imparted by the steel media to the substrate in earlier sections, it was presumed that the steel media would have superior incorporation of the alumina powder. Figure 20 shows representative SEM images of the alumina layer (indicated by purple arrows) on the AA2024 substrate using steel media. Both the 0.5- and 1-h treatment times exhibited large porosity in the alumina layer, as indicated by the dotted arrows in Fig. 20. The 0.5-h layer also shows substantial cracks (red dashed arrow in left-hand image of Fig. 20) that are generally not present in the 1-h alumina layer. However, the alumina layer produced by the 1-h treatment with steel media is markedly thinner than that of the 0.5-h treatment. Comparing the thickness between the crack and the substrate in the 0.5-h micrograph (Fig. 20, left-hand side), it is possible that as the treatment time increases, segments of the alumina layer are fragmented along the cracks, leaving behind only the section closest to the substrate. No cracks were observed in the substrate, contrary to the use of coarse powder as in the previous section.

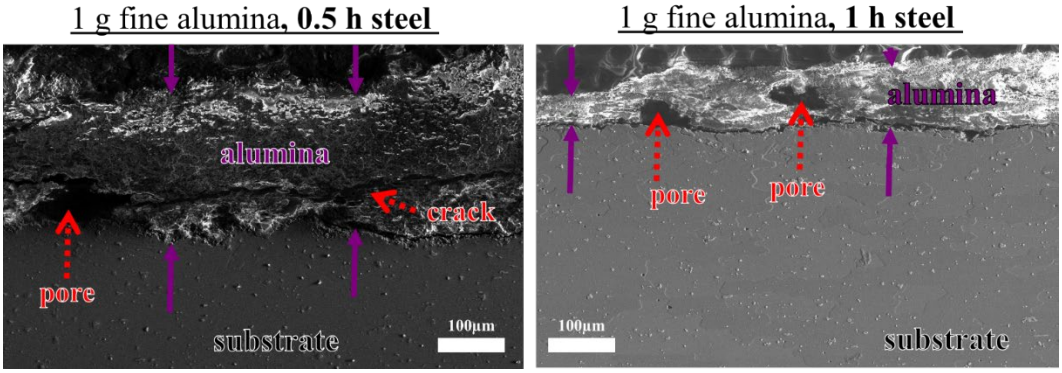

Fig. 20 SEM images of alumina surface layers on AA2024 substrate for SMASH steel media, alumina layer is indicated by purple arrows. Defects (pores and cracks) are indicated by red dashed arrows.

Comparing the effect of the SMASH treatment on the substrate, with and without the alumina powder, it is clear that the process of building the alumina surface layer consumes the kinetic energy / plastic deformation that was previously put into the substrate. Figure 21 shows the significant grain refinement from plastic deformation in the substrate during the SMASH treatment without alumina powder in the system (left-hand side) vis à vis the same treatment time and media with 1 g of alumina powder added. There is no observed grain refinement in the system with the alumina powder.

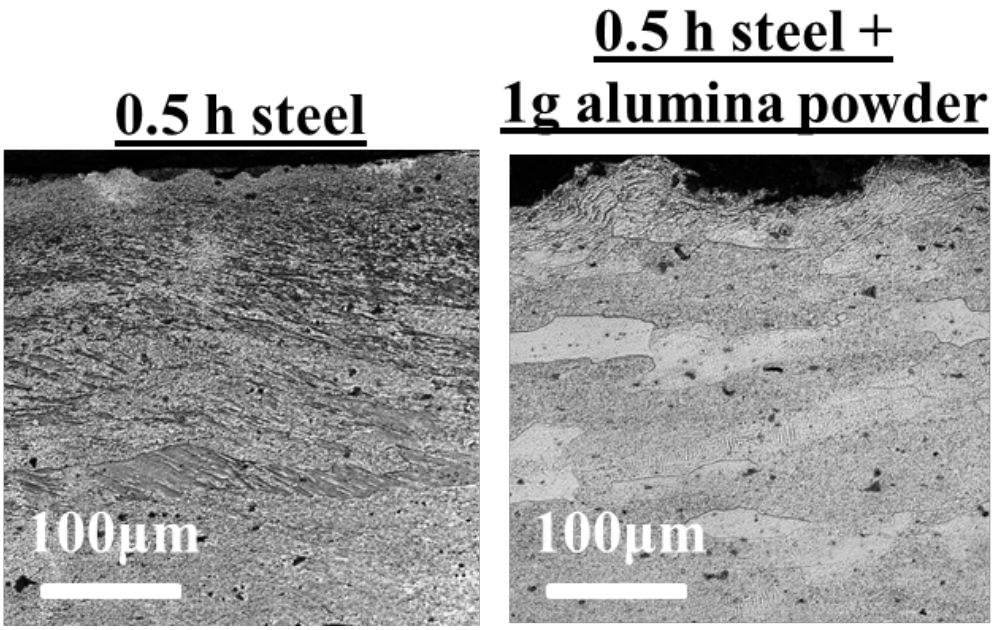

Fig. 21 Comparison of same SMASH processing condition (0.5 h, steel media, AA2024 substrate), with and without alumina surface layer

An improvement in the alumina surface layer was found in switching to the alumina media (shot and vial) from the steel media. Again, 1 g of fine (–325 mesh) alumina powder was added to the SMASH process, and two different treatment times were evaluated, 2 and 4 h. Representative SEM images of these processes are shown in Fig. 22, with the shorter process time on the left-hand side.

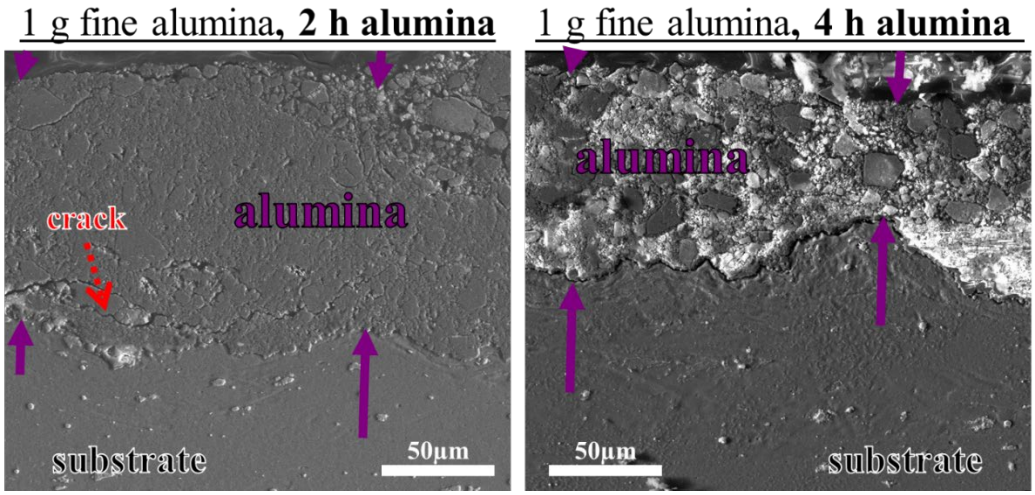

Fig. 22 SEM images of alumina surface layers on AA2024 substrate for SMASH alumina media, alumina layer, is indicated by purple arrows. Defects (pores and cracks) are indicated by red dashed arrows.

Examining the alumina layer itself, both the 2- and 4-h processes had dense compacted powder layers (Fig. 23). A wide distribution of particle sizes is observed in both cases (note that the initial powder size of the alumina is –325 mesh, or particles sizes less than 44 μm). The maximum size of the powder is larger than the width of the images in Fig. 23. In the lower-magnification image (Fig. 22), including the substrate, some larger particles are visible, but most are significantly smaller than the maximum allowable size of the mesh. Given the contamination observed from the alumina media SMASH processes, without any added alumina powder it is likely some part of this distribution of particles is also from contamination from the alumina vial and alumina shot. The right-hand image of Fig. 23 is of a region of alumina contamination in a SMASH process with alumina media but no added alumina powder. The particle size of the "break-off" alumina of the vial and shot appears to comprise all particles smaller than about 10 μm.

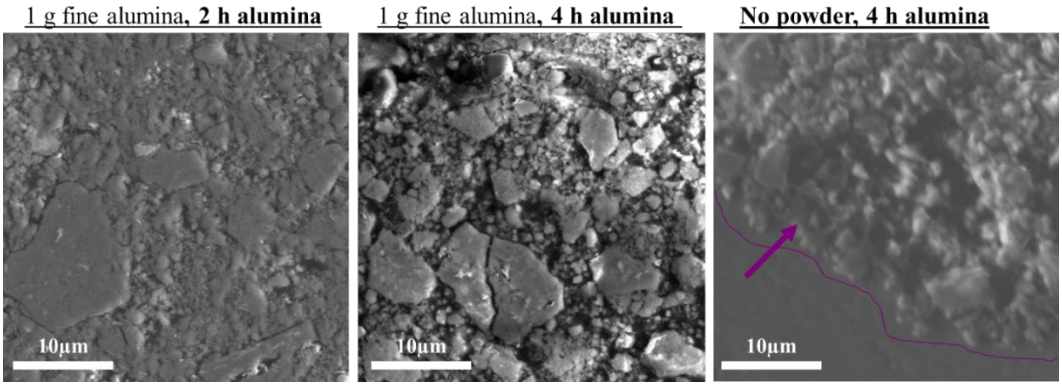

Fig. 23 SEM images of alumina layer only. Amount of powder used and processing time defined across the top. All are with alumina SMASH media.

The viability of the alumina contamination as an alumina surface layer is considered, as the amount of alumina pickup from the vial and shot was considerable in the 4-h SMASH treatment. Figure 24 compares an SEM image of the alumina at the surface of this 4-h SMASH treatment (right hand side) with that of the purposeful alumina-powder-added 4-h treatment to produce a surface layer. While a concentration of alumina at the surface exists, it is naturally a much thinner layer than the purposeful surface coating from added alumina powder. Additionally, the surface suffers from considerable areas where no significant buildup of alumina powder occurs as well as areas where regions of alumina were removed from the surface under continuation of the SMASH impact process (Fig. 24, far right corner).

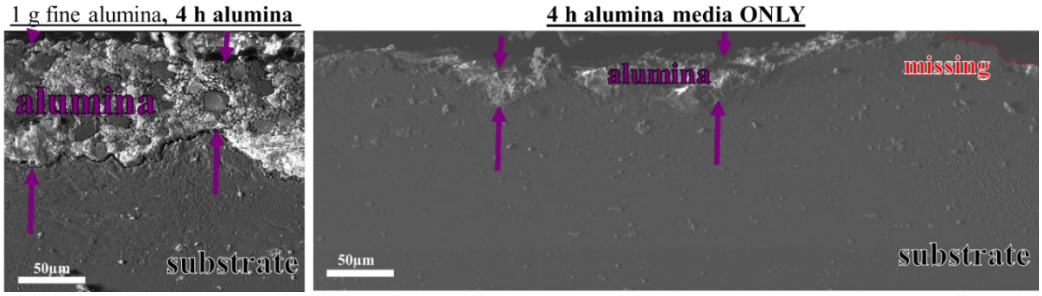

Fig. 24 SEM images of alumina surface layers on AA2024 substrate for SMASH alumina media, (left) with added powder and (right) alumina from contamination

4.3.3 Alumina Color

An interesting macroscopic result was observed for the alumina layers produced with steel media: The color of the alumina layer was black, rather than the initial white powder color. Figure 25A shows a photograph of the surface formed on the AA5083 substrate with steel media (top) and alumina media (bottom) with 1-g alumina powder and 0.5-h SMASH treatment. This color change persisted using steel media on both the AA5083 and AA2024 substrates. The initial hypothesis was that there was enough Fe contamination to form an iron oxide of some form. However, EDS mapping of the cross section and the surface (Fig. 26), both show minimal iron. The samples were also examined by X-ray diffraction (XRD) (Fig. 27), and no iron oxide phases were found, only α-Al_2O_3. Possible other explanations for the color change are porosity and defect density; the amount of deformation imparted by the steel media is significantly higher than the alumina media, as evidenced by the grain refinement differences discussed earlier.

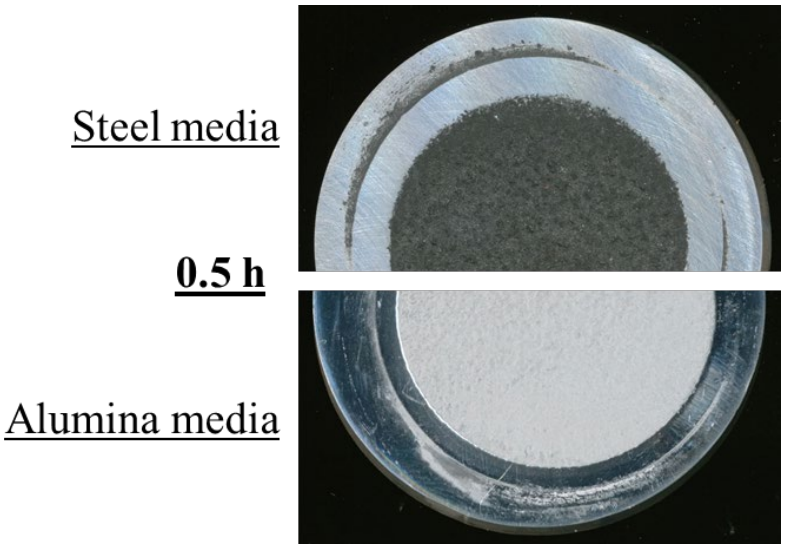

Fig. 25 Photograph of the treated surfaces produced on AA5083 with steel media and alumina media, both with a treatment time of 0.5 h

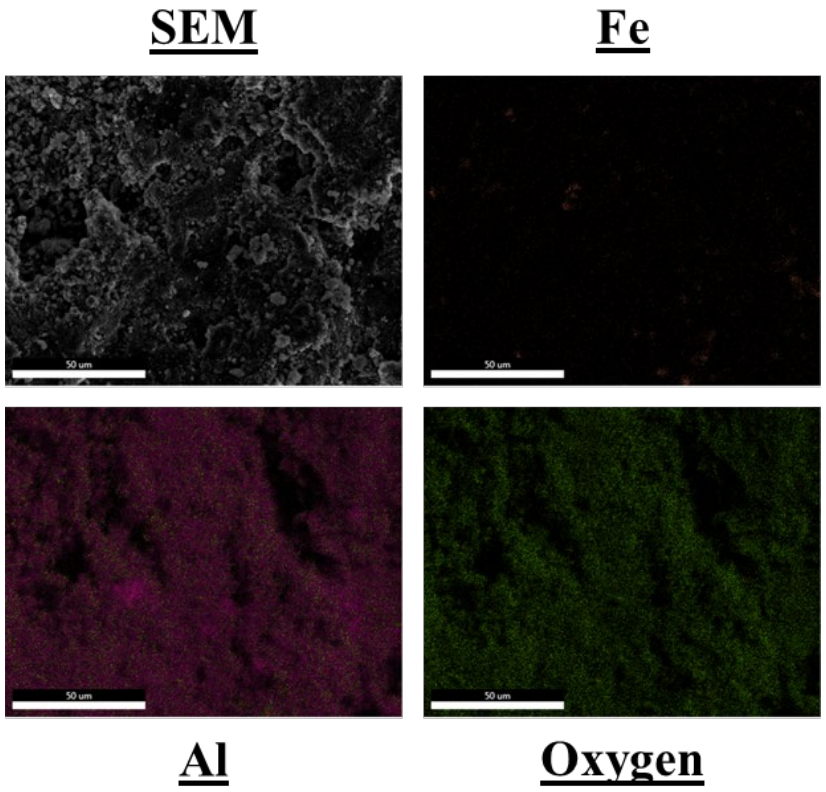

Fig. 26 SEM image and EDS maps of black alumina surface on SMASH-treated AA5083 (0.5 h, steel media)

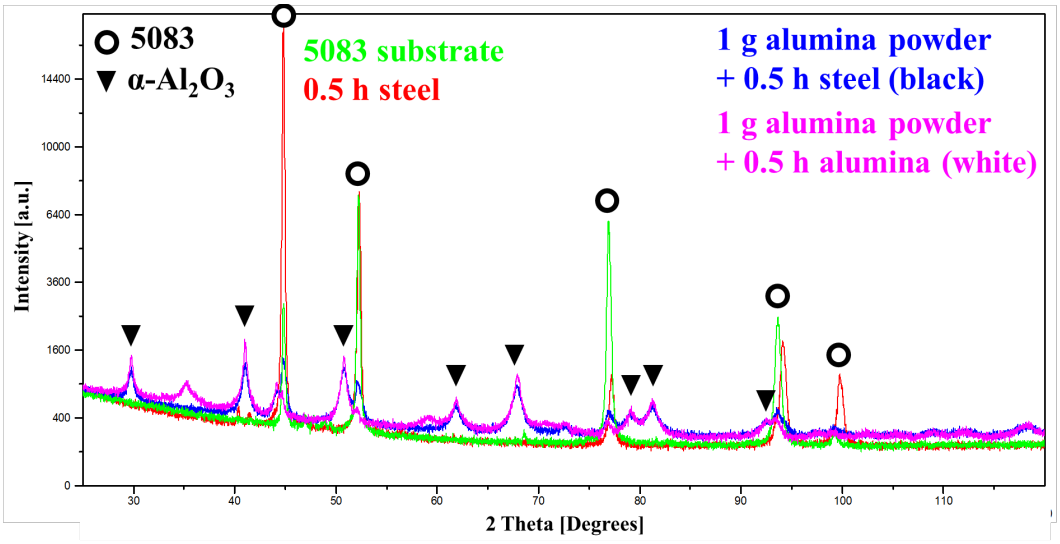

Fig. 27 XRD scans of 5083, various treatments: initial 5083 substrate = green curve; SMASH 0.5 h, steel media = red curve; black alumina surface (1-g alumina powder + 0.5 h, steel media) = blue curve; white alumina surface (1-g alumina powder + 0.5 h, alumina media) = pink curve. Peaks indicating aluminum alloy substrate are marked with an open circle, and peaks matching α-Al2O3 are marked with a black triangle.

4.3.4 Corrosion

Briefly, several of the alumina-coated Al substrates were assessed using potentiodynamic polarization to ensure that the observed behavior was that of the alumina layer (i.e., that it was thick enough) and not the aluminum alloy substrate. An example set of curves is shown in Fig. 28, where the sample with the alumina layer is seen to have distinct behavior from its representative substrate.

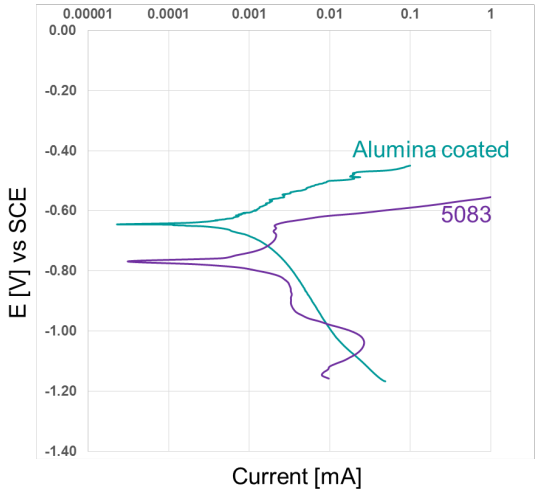

Fig. 28 Potentiodynamic polarization of alumina-coated 5083 (0.5 h, steel media) compared with baseline 5083 substrate

4.3.5 Alumina Surface Layer Summary

- Alumina layers of varying thickness (up to 100 µm) and homogeneity were produced across several processing parameters. Layers were composed of agglomerated alumina powder having a distribution of particle sizes.
- Smaller-mesh powder was more effective; coarse powder produced cracks in the substrate.
- Alumina media was more effective than steel at producing a dense coating.
- Black alumina coatings were observed in some conditions using steel media.

5. Conclusions and Implications for Future Research

5.1 Conclusions

This limited scope project had two major tasks: 1) examining the impact of the SMASH process of the microstructure of an aluminum alloy substrate and its subsequent corrosion response and 2) determining the feasibility of using

mechanical means to engender an alumina layer on the surface of an aluminum alloy substrate. Detailed conclusions can be found in Sections 4.1.4 and 4.2.4 for the two alloys examined in Task 1, and in Section 4.3.5 for Task 2.

Briefly, the SMASH treatment produced grain refinement and an increase in hardness for a variety of process parameters in both substrates. The chemical distribution was altered somewhat, with varying results on the corrosion response. In AA2024, despite reducing the size of intermetallic phases and inducing significant chemical contamination on the surface, the differences in aqueous corrosion response were minimal; however, the exfoliation corrosion response deteriorated significantly due to the grain refinement. In AA5083 the substrate chemistry was changed substantially at the surface, and the corrosion response is still under investigation due to the number of changes vis à vis the baseline.

Surface layers of alumina were produced on both aluminum alloy substrates and through a range of process parameters. The alumina media was more effective than steel at producing dense coatings. Interestingly, the steel media, in some process intervals, produced a black alumina coating. The majority of the alumina layers were in excess of 20 μm, with some approaching 100 μm.

5.2 Future Research

The formed alumina surface layers are far thicker than necessary according to MIL-A-8625F. It is likely that substantially less powder can be used in the process and still achieve a complete alumina surface later. The reduction in powder may significantly improve the density of the layer, the mixing into the substrate, and decrease the processing time, as less impact energy will be consumed by alumina–alumina particle interactions.

As this was a limited scope program, the main tasks were to examine the feasibility of producing an alumina layer through this method. Now that several layers have been produced, next steps would be to evaluate the adhesion of the alumina layer to the substrate and quantify the surface characteristics of both the SMASH-treated substrates and the SMASH-created alumina layers in conjunction with the adhesion of additional parts of standard coatings packages.

As more and more applications require high loads and/or elevated temperatures, the performance of aluminum alloys under static and cyclic loads become more and more crucial. Thus the fatigue performance is also of interest, especially since it is well-known that mechanical surface treatments (e.g., shot peening) are effective methods for prolonging fatigue life. The compressive residual stresses induced by impact from the milling media work in conjunction with the work-hardened layer

to hinder fatigue crack initiation and propagation. For example, an enhanced fatigue lifetime was linked to cracks being initiated in the interior instead of the surface of a gradient nanostructured surface layer in steel, something that was attributed to the suppression of slip bands (surface extrusions and intrusions) during fatigue.[41] For the current aluminum alloys, enhanced fatigue resistance accompanied by the suppressed surface-mode fracture is expected with SMAT/SMASH processing.

The surfaces of the SMASH plates are presumably under a state of compressive stress compared with the underlying material. Thus, characterizing the distribution of stress whether through XRD analysis or nanoindentation testing could help to explain some of the phenomena observed (e.g., the Mg-depleted layer beneath the SMASH surface). It is possible that the compressive stress profile could have a direct correlation to the chemical distribution in the first 50 μm of the surface.

6. References

1. MIL-A-8625F. Anodic coatings for aluminum and aluminum alloys. Lakehurst (NJ): Naval Air Warfare Center; 1993 Sep 10.

2. Goueffon Y, Arurault L, Maru C, Tonon C, Guigue P. Black anodic coatings for space applications: study of the process parameters, characteristics and mechanical properties. Journal of Materials Processing Technology. 2009;209(11):5145–5151.

3. Buchheit RG, Grant RP, Hlava PF, Mckenzie B, Zender GL. Local dissolution phenomena associated with S phase (Al2CuMg) particles in aluminum alloy 2024-T3. Journal of the Electrochemical Society. 1997;144(8):2621–2628.

4. Murer N, Missert NA, Buchheit RG. Finite element modeling of the galvanic corrosion of aluminum at engineered copper particles. Journal of the Electrochemical Society. 2012;159(6):C265–C276.

5. Fontana MG. Corrosion engineering. New York (NY): Tata McGraw-Hill Education; 2005.

6. Boag A, Hughes AE, Wilson NC, Torpy A, MacRae CM, Glenn AM, Muster TH. How complex is the microstructure of AA2024-T3? Corrosion Science. 2009;51(8):1565–1568.

7. Schneider O, Ilevbare GO, Scully JR, Kelly RG. In situ confocal laser scanning microscopy of AA2024-T3 corrosion metrology: II. Trench formation around particles. Journal of the Electrochemical Society. 2004;151(8):B465–B472.

8. Zhang R, Birbilis N, Knight S, Holtz RL. A survey of sensitization in 5xxx series aluminum alloys. Corrosion. 2015;72(2).

9. Zhang R, Gupta RK, Davies CHJ, Hodge AM, Tort M, Xia K, Birbilis N. The influence of grain size and grain orientation on sensitization in AA5083. Corrosion. 2016;72(2):160–168.

10. Kus E, Mansfed F, Lee Z, Nutt SR. A comparison of the corrosion behavior of nanocrystalline and conventional Al 5083 samples. Corrosion. 2006;62(2):152–161.

11. Zhao Y, Polyakov, Mecklenburg M, Kassner ME. The role of grain boundary plane orientation in the β phase precipitation of an Al–Mg alloy. Scripta Materialia. 2014;89:49–52.

12. Scotto D'Antuono D, Gaies J, Golumbfskie W, Taheri ML. Grain boundary misorientation dependence of β phase precipitation in an Al–Mg alloy. Scripta Materialia. 2014;76:81–84.

13. Tan L, Allen TR. Effect of thermomechanical treatment on the corrosion of AA5083. Corrosion Science. 2010;52(2):548–554.

14. Davenport AJ, Yuan Y, Ambat R, Connolly BJ, Strangwood M, Afseth A, Scamans GM. Intergranular corrosion and stress corrosion cracking of sensitised AA5182. Materials Science Forum. 2006;519-520:641–646.

15. Darling KA, Tschopp MA, Roberts AJ, Ligda JP, Kecskes LJ. Enhancing grain refinement in polycrystalline materials using surface mechanical attrition treatment at cryogenic temperatures. Scripta Materialia. 2013;69(6):461–464.

16. Murdoch HA, Darling KA, Roberts AJ, Kecskes L. Mechanical behavior of ultrafine gradient grain structures produced via ambient and cryogenic surface mechanical attrition treatment in iron. Metals. 2015;5(2):976–985.

17. Ralston KD, Birbilis N. Effect of grain size on corrosion: a review. Corrosion. 2010;66(7).

18. Ralston KD, Birbilis N, Davies CHJ. Revealing the relationship between grain size and corrosion rate of metals. Scripta Materialia. 2010;63(12):1201–1204.

19. Miyamoto H. Corrosion of ultrafine grained materials by severe plastic deformation: an overview. Materials Transactions. 2016;57(5):559–572.

20. Ralston KD, Fabijanic D, Birbilis N. Effect of grain size on corrosion of high purity aluminium. Electrochimica Acta. 2011;56(4):1729–1736.

21. Song D, Ma AB, Jiang JH, Lin PH, Shi J. Improving corrosion resistance of pure Al through ECAP. Corrosion Engineering, Science and Technology. 2011;46(4):505–512.

22. Eizadjou M, Fattahi H, Talachi AK, Manesh HD, Janghorban K, Shariat MH. Pitting corrosion susceptibility of ultrafine grains commercially pure aluminum produced by accumulative roll bonding process. Corrosion Engineering, Science and Technology. 2012;47(1):19–24.

23. Esquivel J, Murdoch HA, Darling KA, Gupta RK. Excellent corrosion resistance and hardness in Al alloys by extended solid solubility and nanocrystalline structure. Materials Research Letters. 2018;6(1):79–83.

24. Sharma MM, Ziemian CW. Pitting and stress corrosion cracking susceptibility of nanostructured Al-Mg alloys in natural and artificial environments. Journal of Materials Engineering and Performance. 2008;17(6):870–878.

25. Sikora E, Wei XJ, Shaw BA. Corrosion behavior of nanocrystalline bulk Al-Mg-based alloys. Corrosion. 2004;60(4):387–398.

26. Argade GR, Kumar N, Mishra RS. Stress corrosion cracking susceptibility of ultrafine grained Al–Mg–Sc alloy. Materials Science and Engineering: A. 2013;565:80–89.

27. op't Hoog C, Birbilis N, Estrin Y. Corrosion of pure Mg as a function of grain size and processing route. Advanced Engineering Materials. 2008;10(6):579–82.

28. Brunner JG, Birbilis N, Ralston KD, Virtanen S. Impact of ultrafine-grained microstructure on the corrosion of aluminum alloy AA2024. Corrosion Science. 2012;57:209–214.

29. Bousquet E, Poulon A, Puiggali M, Devos O. Relationship between microstructure, microhardness and corrosion sensitivity of an AA2024-T3 friction stir welded joint. Corrosion Science. 2011;53(9):3026–3034.

30. Sun Q, Han Q, Xu R, Zhao K, Lie J. Localized corrosion behavior of AA7150 after ultrasonic shot peening: corrosion depth vs. impact energy. Corrosion Science. 2018;130:218–230. Supplement C.

31. Goswami R, Spanos G, Pao PS, Holtz RL. Precipitation behavior of the ß phase in Al-5083. Materials Science and Engineering: A. 2010;527(4–5):1089–1095.

32. Dai K, Shaw L. Comparison between shot peening and surface nanocrystallization and hardening processes. Materials Science and Engineering: A. 2007;463(1–2):46–53.

33. Ortiz AL, Tian J-W, Shaw LL, Liaw PK. Experimental study of the microstructure and stress state of shot peened and surface mechanical attrition treated nickel alloys. Scripta Materialia. 2010;62(3):129–132.

34. Murdoch HA, Labukas, JP, Roberts, AJ, Darling KA. Controlling surface chemistry to deconvolute corrosion benefits derived from SMAT processing. JOM. 2017:69(7):1170–1174.

35. ASTM G34-01(2013). Standard test method for exfoliation corrosion susceptibility in 2XXX and 7XXX series aluminum alloys (EXCO test). West Conshohocken (PA): ASTM International; 2013.

36. Kumar Singh A, Ghosh S, Mula S. Simultaneous improvement of strength, ductility and corrosion resistance of Al2024 alloy processed by cryoforging followed by ageing. Materials Science and Engineering: A. 2016;651:774–785. Supplement C.

37. Mirzaei M, Roshan MR, Jenabali Jahromi SA. Microstructure and mechanical properties relation in cold rolled Al 2024 alloy determined by X-ray line profile analysis. Materials Science and Engineering: A. 2015;620:44–49.

38. Estrin Y, Vinogradov A. Extreme grain refinement by severe plastic deformation: a wealth of challenging science. Acta Materialia. 2013;61(3):782–817.

39. Goswami R, Pao PS, Qadri SB, Holtz RL. Severe plastic deformation induced sensitization of cryo-milled nanocrystalline Al-7.5 Mg. Metallurgical and Materials Transactions A. 2014;45(6):2894–2898.

40. Gupta RK, Favijanic D, Zhang R, Birbilis N. Corrosion behavior and hardness of in situ consolidated nanostructured Al and Al–Cr alloys produced via high-energy ball milling. Corrosion Science. 2015;98:643–650.

41. Zhang K, Wang Z, Lu K. Enhanced fatigue property by suppressing surface cracking in a gradient nanostructured bearing steel. Materials Research Letters. 2017;5(4):258–266.

List of Symbols, Abbreviations, and Acronyms

AA	aluminum alloy
Al	aluminum
Cr	chromium
Cu	copper
DOD	US Department of Defense
DOS	degree of sensitization
EBSD	electron backscatter diffraction
ECAE	Equal Channel Angular Extrusion
EDS	energy dispersive spectroscopy
Fe	iron
Mg	magnesium
Mn	manganese
NaCl	sodium chloride
NAMLT	Nitric Acid Mass Lost Test
NASA	National Air and Space Administration
OCP	open circuit potential
SCE	saturated calomel electrode
SEM	Scanning Electron Microscopy
SMASH	Surface Mechanical Alloying for Specialized Heterogeneity
SMAT	Surface Mechanical Attrition Treatment
SPD	severe plastic deformation
XRD	X-ray diffraction

1 (PDF)	DEFENSE TECHNICAL INFORMATION CTR DTIC OCA
1 (PDF)	CCDC ARL FCDD RLD CL TECH LIB
1 (PDF)	GOVT PRINTG OFC A MALHOTRA
1 (PDF)	CCDC ARL FCDD RLW MF H MURDOCH